
Electromagnetic Images of the South and Central American Subduction Zones

4

Heinrich Brasse

Abstract

Current and fossil plate margins offer some of the most rewarding targets for geophysical studies. Particularly, the fluid/melt cycle in subduction zones continues to be of major interest for seismological as well as deep electromagnetic (EM), specifically magnetotelluric investigations. In this contribution we describe a number of experiments which have been conducted in several ocean-continent convergence zones around the world, with a focus on the Andes and Central America, respectively. Zones of potentially high electrical conductivity range from bending-related faulting near the outer rise, the subduction channel at the tip of the continental plate, the dehydration-hydration cycles in and above the downgoing plate, the assumed melting of the asthenospheric wedge to the rise of melts toward the volcanic arc and the magma chambers beneath the volcano edifices. Further targets include fault zones in the forearc, accommodating tensional stress, as well as hydrothermal and mineral deposits, to mention a few. The following chapters emphasize on a variety of structures along continental margins and show the potential of deep EM in this geodynamic setting.

4.1 Introduction

It is one of the wonders of geoscience that volcanic ranges where hot, molten material reaches the surface, are often located at subduction zones in which cold oceanic lithosphere is subducted. This enigma has been resolved during the last decades by numerous geological, geophysical, mineralogical and petrological studies: As the downgoing plate reaches larger

depth, i.e., higher temperatures and pressures, mineral-bound water is released in a succession of dehydration/hydration reactions. At certain depths, the released water leads to lowering of the solidus and partial melting of mantle material of the overriding plate. The melt then rises – perhaps with some intermediate storage at crustal density boundaries – to the surface, where it erupts at arc volcanoes. These processes are described, e.g., by Schmidt and Poli (1998), see also Fig. 4.1.

They should lead to distinct geophysical anomalies, particularly to low seismic velocity and high electrical conductivity (low resistivity) zones. Electrical conductivity σ , measured in S/m (Siemens per meter), of rocks is normally low at crustal or even upper

H. Brasse (✉)
Freie Universität Berlin, Fachrichtung Geophysik,
12249 Berlin, Germany
e-mail: heinrich.brasse@fu-berlin.de

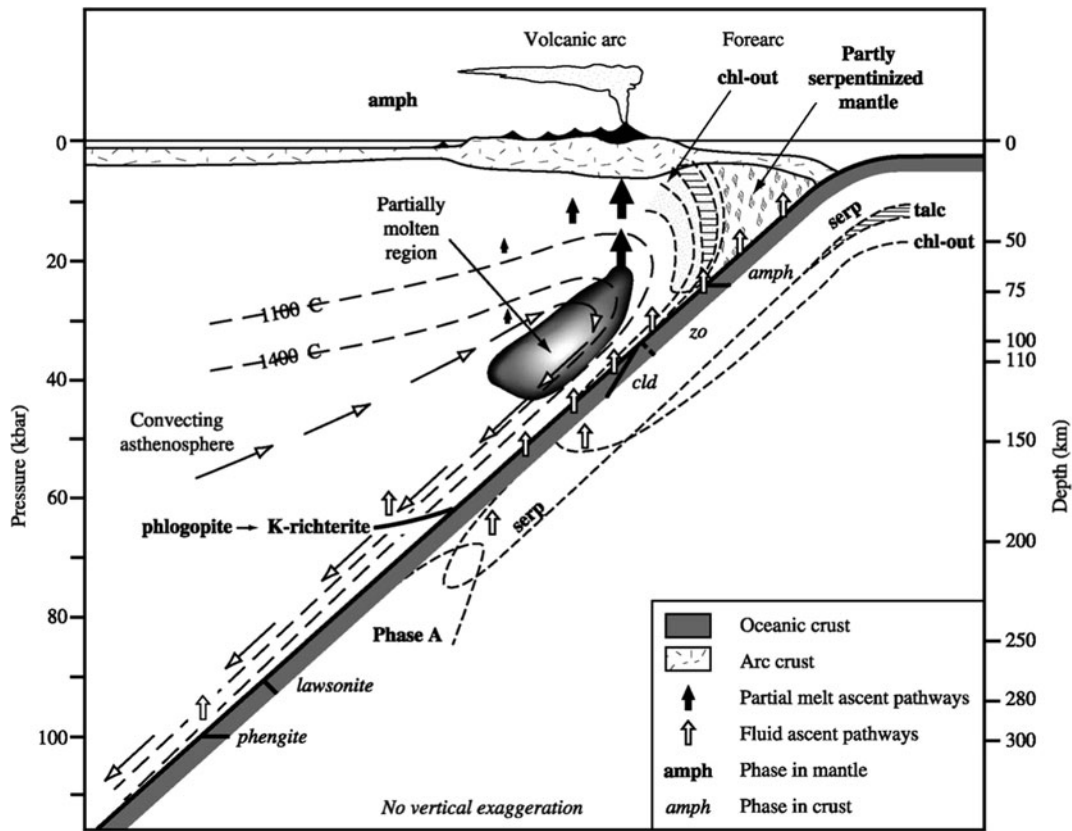


Fig. 4.1 The fluid-melt cycle in subduction zones (Schmidt and Poli 1998)

mantle temperatures. When metal or fluid phases come into play, a dramatic increase of conductivity is usually observed. Thus, investigation of the conductivity structure may be a valuable tool in the exploration of subduction zones, where fluids and melts play a significant role. And, indeed, numerous geophysical images in various parts of the world showing these effects have been presented in the past. Often, the resulting models do not image the complete fluid/melt cycle as evident from Fig. 4.1, but only aspects thereof, and reveal surprising aspects which were not known before.

The EMSLAB amphibious (onshore-offshore) electromagnetic experiment was intended to study the resistivity structure of the Cascadia subduction zone, where the Juan de Fuca plate subducts beneath the North American continent. Instruments were deployed along the Lincoln line in the state of Oregon with a seaward extension across the trench. Early 2-D forward and inversion models (Jiracek et al. 1989, Wannamaker

et al. 1989) already showed low-resistivity zones (with resistivity $\rho = 1/\sigma$, measured in Ωm) on top of the subducting plate and beneath the volcanic range of the High Cascades. Later, various modeling and inversion attempts were conducted by the Russian EM community (Varentsov et al. 1996, Vanyan et al. 2002); from these studies the final model EMSLAB III of Vanyan et al. (2002) is shown in Fig. 4.2. The geometry of model domains was derived from seismological and gravity investigations, and resistivity was allowed to vary within these preset domains. Again, a low-resistivity zone is evident above the Juan de Fuca plate, extending to a depth of approx. 40 km. It is not clear yet, if this HCZ (high-conductivity zone) is related to the subduction channel or to the directly overlying zone where hydration (serpentinization) occurs again. A moderate, dike-shaped conductor is modeled beneath the High Cascades (HC in Fig. 4.2), which is rooted in the asthenosphere of the overriding plate. Interestingly, in the lower crust the conductor broadens

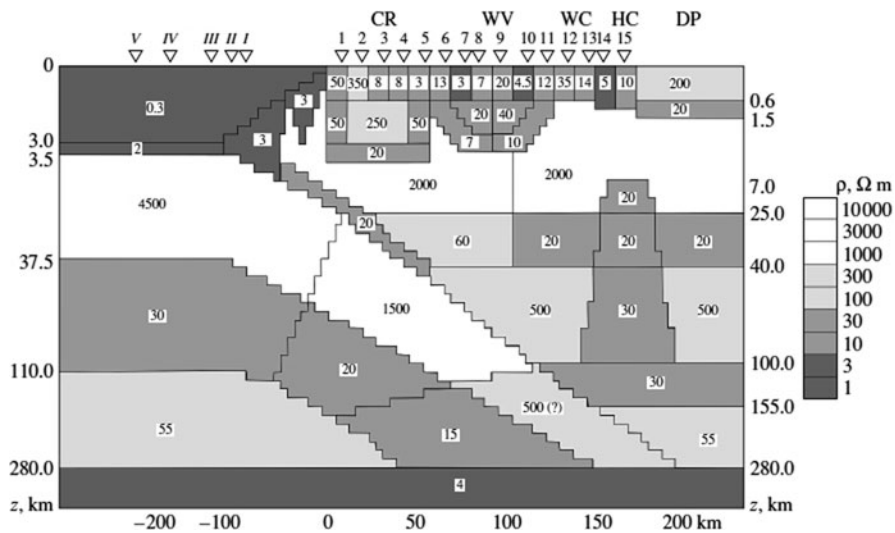


Fig. 4.2 Resistivity model of the Cascadia subduction zone (Vanyan et al. 2002). Note the non-linear depth scale

and extends into the forearc until the Willamette Valley and into the backarc beneath the Deschutes Basin (WV and DP in Fig. 4.2).

A HCZ beneath at least some of the High Cascades volcanoes was also imaged by Patro and Egbert (2008) with 3-D inversion of magnetotelluric impedance data from the USArray experiment, using broadly distributed stations from the northwestern United States. A very distinct anomaly is observed by Hill et al. (2009) below Mount St. Helens and an obvious connection towards Mount Adams. Although there is some debate about the cause of the enhanced conductivity, the most probable source seems to be partial melt.

Studies restricted to land measurements alone may often not image a HCZ above the slab or associated with the subduction channel, as was pointed out by Evans et al. (2002). And indeed, apart from the Cascadia models mentioned above, such a structure has never been observed on the basis of onshore data, neither in Canadian Cascadia (Soyer and Unsworth 2006) nor in Japan or New Zealand (Wannamaker et al. 2009). However, at the Mexican margin and farther inland, Jödicke et al. (2006) resolved a distinct anomaly above the subducting plate which they attribute to dewatering of the slab.

Apart from the investigation of Mount St. Helens mentioned above, arc volcanoes seem to be a difficult target for a detailed passive EM study, particularly due to often rugged topography, the shielding effect of hydrothermal systems, and the limited spatial

extent of possible magma chambers and the feeder dike; see e.g. the 3-D model study at Merapi volcano, Indonesia (Müller and Haak 2004) or the combined MT/self-potential work at volcanoes in Japan (Aizawa et al. 2009). More promising targets seem to be large caldera systems, e.g., the Taupo volcanic zone in New Zealand (Heise et al. 2010).

4.2 Basic Principles of the Magnetotelluric Method

In this section an overview of the magnetotelluric method is given and the terms and concepts necessary to understand the following are briefly explained. For a comprehensive overview the reader is referred to the literature, e.g., Simpson and Bahr (2005) or Zhdanov (2009).

Electromagnetic (EM) exploration comprises a wide variety of sounding methods. While active methods, which involve the usage of transmitters, are primarily utilized in the exploration of near-surface structures, only passive methods may be employed for sounding of Earth's deeper crust and upper mantle.¹ For periods T larger than roughly 1 s, energy

¹ Hybrid cases are the so-called VLF (very low frequency) and RMT (radio magnetotelluric) methods which use the radiation

is provided by the time-varying solar wind, which carries a frozen magnetic field from the surface of the sun. Particles of the solar wind – primarily protons – interact with the Earth’s magnetosphere and lead to variations of the magnetic field over a wide period range. Additionally, ionization of the ionosphere by ultraviolet solar radiation leads to large-scale current systems which in turn influence the magnetic field. For short periods $T < 1$ s, electromagnetic radiation (“atmosferics” or “sferics”) from lightning strokes provides the source. A particular case are the Schumann resonances, standing waves in the waveguide formed by the ionosphere and Earth’s surface, with frequencies $f \approx 7.8, 14.1, 20.3, \dots$ Hz. Sprites, elves, blue jets and other phenomena associated with the upward discharge of thunderclouds are perhaps not frequent enough to act as a near-permanent source, as required for passive EM sounding; the same probably holds also for whistlers.

Altogether, a wide period range, generally from $T \approx 10^{-4}$ s to $T \approx 10^4$ s is available for EM sounding. The fields diffuse into the conducting earth, where they induce a current system which in turn induces a secondary magnetic field. A superposition of primary and secondary magnetic and electric fields is then measured at the surface. A scale length for the induction process in a homogeneous half space is the depth of penetration or skin depth

$$\delta = \sqrt{\frac{2}{\mu\omega\sigma}} \approx 0.503\sqrt{\rho T} \text{ [km]} \quad (4.1)$$

with μ denoting magnetic permeability of free space (the relative permeability of the Earth may be set to 1 in most cases), ω angular frequency, σ electrical conductivity, and electrical resistivity $\rho = 1/\sigma$; at depth δ the magnitude of the field has decayed to $1/e$ of its surface value. σ is measured in S/m, while Ωm is the unit of ρ .

In the magnetotelluric sounding method (MTS) horizontal electric and magnetic fields are measured at the surface of the earth. In geomagnetic depth sounding (GDS) the vertical magnetic field is related to the horizontal magnetic field, while in magneto-variational sounding (MVS) the magnetic fields at

different locations are compared. The fields have to fulfill the quasi-homogeneous approach, i.e., their spatial structure may be approximated as a plane wave. This is certainly not the case for the ionospheric current systems, e.g., the Sq (solar quiet) current and the polar and equatorial electrojets (PEJ and EEJ).²

The magnetotelluric impedance³ \mathbf{Z} is defined as a complex transfer function between horizontal electric and horizontal magnetic fields in the frequency (or period) domain:

$$E_x(T) = Z_{xx}(T)B_x(T) + Z_{xy}(T)B_y(T) \quad (4.2)$$

$$E_y(T) = Z_{yx}(T)B_x(T) + Z_{yy}(T)B_y(T), \quad (4.3)$$

where x, y, z denote Cartesian, geomagnetic coordinates, E is the electric field, B geomagnetic induction and T period.

For an one-dimensional (1-D) subsoil the main diagonal of the impedance tensor vanishes and $Z_{xy} = -Z_{yx}$. In a 2-D environment a coordinate system may be found by rotation of \mathbf{Z} with the strike angle α so that the main diagonal (in rotated coordinates) vanishes again, but now $Z_{xy} \neq -Z_{yx}$. In E-Polarization or TE mode (electric field \parallel strike) a vertical magnetic field arises, while the vertical electric field in B-Polarization or TM mode (magnetic field \parallel strike) is almost never measured. In 3-D, an assignment of TE and TM modes is no longer possible. Interpretation is often complicated by “static shift” or galvanic effects, the parallel shifting of apparent resistivity curves $\rho_a(T)$ due to small-scale, near-surface heterogeneities without affecting the phase $\phi(T)$. A distortion-free measure of the impedance is the phase tensor (Caldwell et al. 2004).

The tipper $\mathbf{W} = (W_x, W_y)^t$ (with t denoting transpose) is defined as a complex transfer function between vertical and horizontal magnetic fields (Schmucker 1970):

$$B_z(T) = W_x(T)B_x(T) + W_y(T)B_y(T). \quad (4.4)$$

² If the spatial structure of the field is known, an extension of the methods described above may be used to estimate conductivity of the Earth.

³ The impedance is defined here via the magnetic induction B as is common in MT, yielding an unit of m/s. By replacing induction B with the magnetic field H the expected unit of Ω is obtained.

from distant transmitters for communication with submarines and LF radio stations, respectively.

It is conveniently displayed as an “induction arrow” or “induction vector”⁴ for both real and imaginary parts, calculated according to:

$$\mathbf{P}(T) = \text{Re}\{W_x(T)\}\mathbf{e}_x + \text{Re}\{W_y(T)\}\mathbf{e}_y \quad (4.5)$$

$$\mathbf{Q}(T) = \text{Im}\{W_x(T)\}\mathbf{e}_x + \text{Im}\{W_y(T)\}\mathbf{e}_y, \quad (4.6)$$

with \mathbf{e}_x and \mathbf{e}_y as unity vectors in x- and y-direction. If plotted on a map, real arrows point away from conductive zones in a 2-D environment, while imaginary arrows change signs at the period where the real arrow is maximal; this is the so-called *Wiese* convention. Sometimes the real arrow is reversed to make it point towards conductive anomalies; this style is referred to as *Parkinson* convention.

In magneto-variational sounding, magnetic fields at a site are referenced to a remote or base station (Schmucker 1970):

$$B_x(T) = M_{xx}(T)B_x^b(T) + M_{xy}(T)B_y^b(T) \quad (4.7)$$

$$B_y(T) = M_{yx}(T)B_x^b(T) + M_{yy}(T)B_y^b(T) \quad (4.8)$$

$$B_z(T) = M_{zx}(T)B_x^b(T) + M_{zy}(T)B_y^b(T) \quad (4.9)$$

with b denoting the base and \mathbf{M} is the magnetic tensor. Often a 1-D base station is not available in the measuring area; then only “inter-station” transfer functions are calculated. Both \mathbf{M} and the tipper \mathbf{W} are practically not affected by static shift.

4.3 Electrical Resistivity Beneath the Andes

The Andes form a circa 8000 km long mountain range where the oceanic Nazca and Antarctic plates subduct beneath the South American continent; the oceanic plates are separated by the Chile Rise as a continuation of the East Pacific Rise. Convergence rate of Nazca-South American plates amounts to currently 6.5 cm/yr (Klotz et al. 2006). At the Chilean margin, convergence is oblique with a direction of $\sim N80^\circ E$. Four

volcanic provinces are identified along the margin: (1) The Northern Volcanic Zone (NVZ) of Colombia and Ecuador, (2) the Central Volcanic Zone (CVZ) in Peru, Bolivia, Argentina and Chile at the western rim of the Altiplano-Puna high plateau, (3) the Southern Volcanic Zone along the border of Argentina and Chile, and (4) the Austral Volcanic Zone (AVZ) south of the triple junction, where volcanism is predominantly occurring on Chilean territory. For the Central Andes volcanism spatially correlates with (relatively) steep subduction of the Nazca plate (Cahill and Isacks 1992), while large volcanic gaps occur in the adjacent regions of sub-horizontal (flat-slab) subduction in Peru and Chile/Argentina. Backarc volcanism occurs in various parts of Bolivia as well as Argentina.

The Peru-Chile Trench shows markedly different characteristics along the margin. In the Central Andes it reaches depths of 8000 m and is almost devoid of sediments due to the hyper-arid climate of the Atacama desert, while the southern trench is dominated by large sedimentary filling as a consequence of abundant rainfall; this can immediately be seen in a topographic/bathymetric map (Fig. 4.3). Depth of the trench slowly decreases from north to south.

In spite of the enormous dimensions of the mountain range and the abundance of geoscientific targets, the Andes remain until today largely undersampled with regard to deep EM sounding. The first observation of an extended high-conductivity zone beneath the Central Andes came from a magnetometer array established by the Carnegie Institution of Washington (Schmucker et al. 1966). Much later, in the eighties and early nineties of last century the Free University of Berlin carried out a magnetotelluric transect over the entire mountain range at approximately $22^\circ S$. This study revealed mid-crustal high-conductivity zones beneath the volcanic arc as well as beneath the Altiplano plateau (Schwarz and Krüger 1997). More recently, the Argentinian flat-slab segment was subject to a study by the universities of Washington and Buenos Aires. A spectacular electrical anomaly (see Fig. 4.4) was detected at large depths of ≥ 100 km and extending to at least 250 km (perhaps more than 400 km), which was attributed to image partial melting associated with the plunging of the Nazca plate (Booker et al. 2004).

⁴ Although the term vector is often used (also in this text), note that, for coupled anomalies the “vectors” can’t simply be added (Siemon 1997).

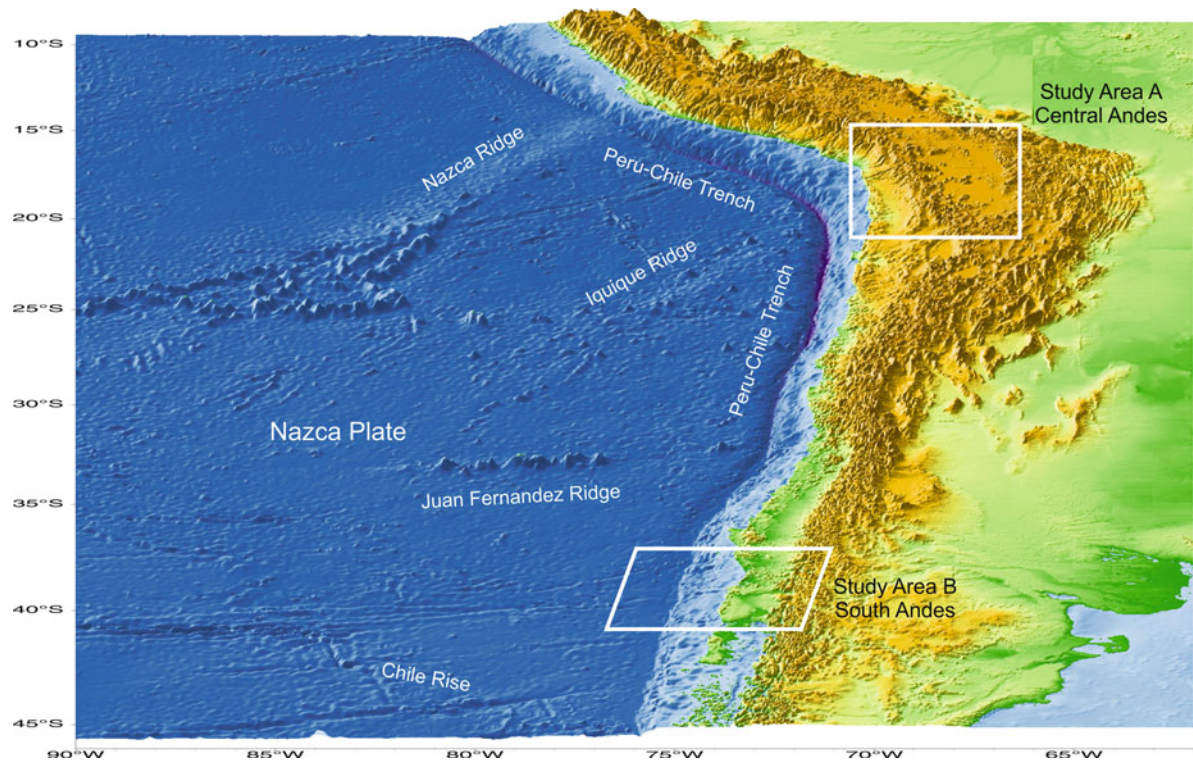


Fig. 4.3 Topographic-bathymetric map of the Central and Southern Andes and the Nazca plate, derived from ETOPO1 data. Note the change of morphology of the trench along the

margin and the widening of the mountain range in the Central Andes (Altiplano-Puna Plateau). Study areas of this contribution are also shown

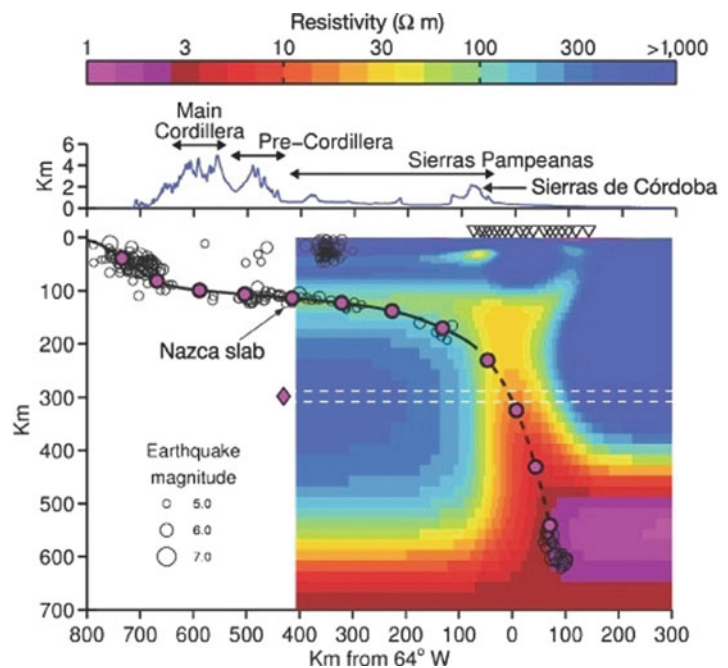


Fig. 4.4 Resistivity model of the Pampean flat-slab segment in Western Argentina, modified from (Booker 2004)

4.3.1 The Central Andes

In the Central Andes of Peru, Chile, Bolivia and Argentina the 1800 km long and up to 350 km wide Altiplano-Puna high plateau, with average elevations of 3800 m in its northern (Altiplano) and 4500 m in its southern part (Puna), has evolved since the late Oligocene; crustal thickness amounts to 70 km (James 1971, Wigger 1994, Yuan et al. 2002, ANCORP Working Group 2003). The causes for uplift are mainly seen in crustal shortening (e.g., Allmendinger et al. 1997, Elger et al. 2005) with perhaps minor contributions from magmatic addition beneath the volcanic arc (Dorbath and Masson 2000) or hydration of the lithospheric mantle (James and Sacks 1999). The uplift is thought to have been triggered by arid to hyperarid climatic conditions prevailing at the central western Andean margin since at least the Miocene (Lamb and Davis 2003), which led in turn to a trench nearly completely devoid of sediments (von Huene et al. 1999). At

the Peru-Chile trench (reaching depths of up to 8 km in the region of the Central Andes) the Nazca plate currently subducts obliquely with an angle of N77°E and a velocity of 6.5 cm/a (Klotz et al. 2006); the angle of subduction is $\sim 25\text{--}30^\circ$ below the plateau (Cahill and Isacks 1992). The active volcanic arc – with individual edifices exceeding heights of 6000 m – developed at the western margin of the plateau.

A large number of long-period magnetotelluric measurements have been conducted along several profiles in the Central Andes. The current synthesis concentrates on transects A, B and C, which all cross the volcanic arc and reach into or traverse the high plateau (Fig. 4.5).

4.3.1.1 The Southern Plateau

At latitude 21°S the southern Altiplano crust in Bolivia is characterized by large, coincident geophysical anomalies, in particular a broad and deep-reaching zone of enhanced conductivity (Fig. 4.6, Soyer and

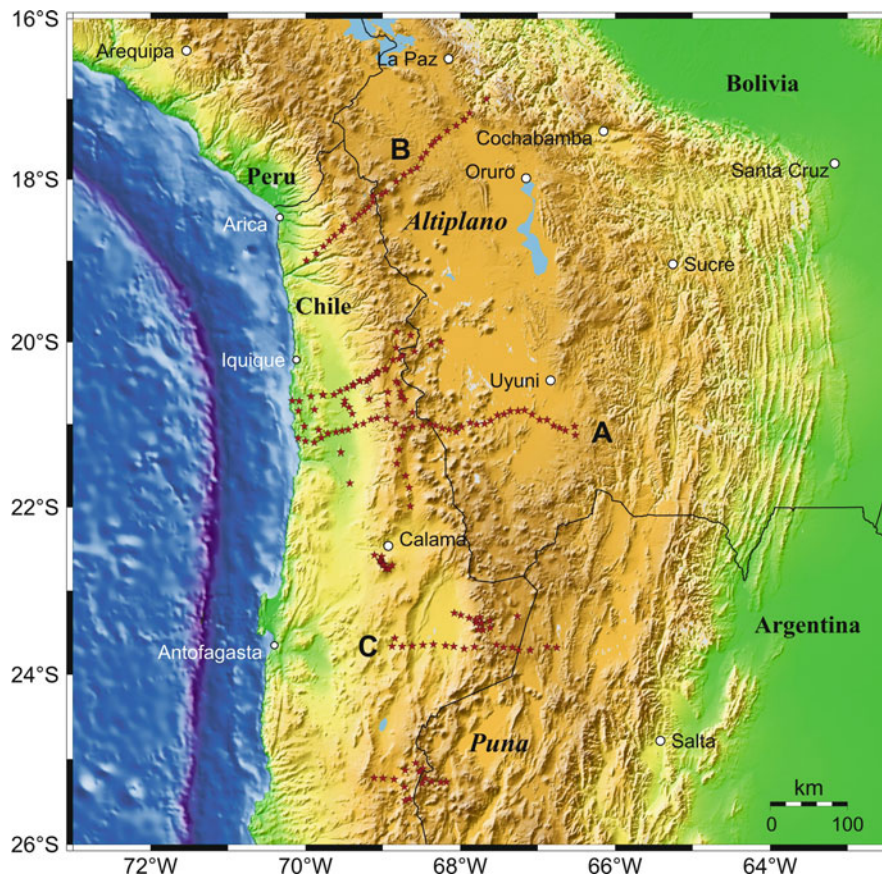


Fig. 4.5 Magnetotelluric sites in the Central Andes. Transects A, B and C are treated in the text

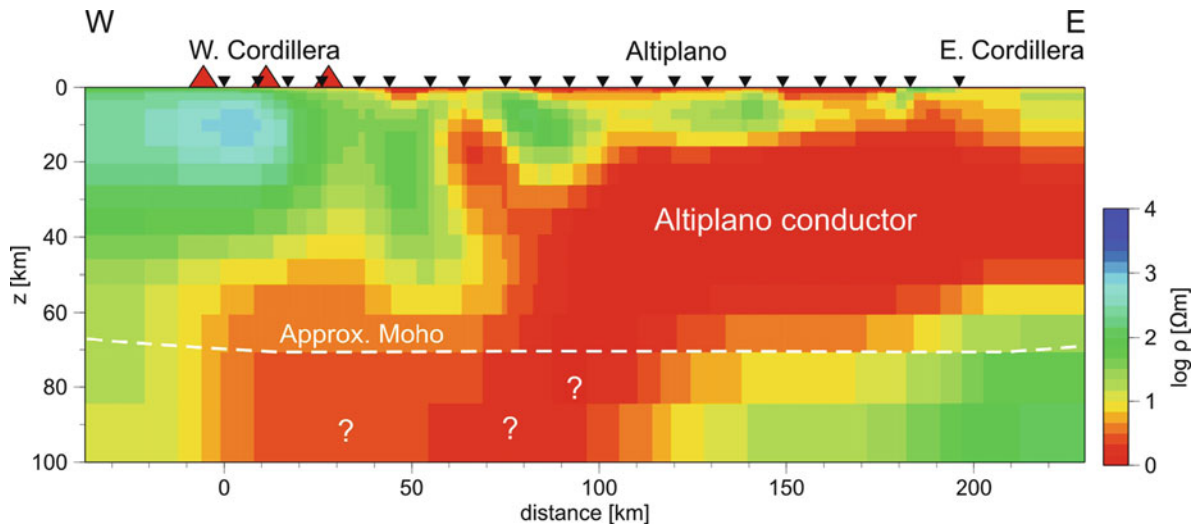


Fig. 4.6 2-D resistivity model of the Western Cordillera and the Southern Altiplano at 21°S

Brasse 2001, Brasse et al. 2002), high attenuation of seismic waves (Haberland et al. 2003) and low velocities (Heit 2005), all hinting at the occurrence of large volumes of partial melt (Schilling et al. 2006). Note that the model in Fig. 4.6 is a new compilation: Whereas in (Brasse et al. 2002) a Gauss-Newton version of the 2-D code of Rodi and Mackie (2001) was applied and only MT impedances were inverted, here tipper data were included and the non-linear conjugate gradient version was employed. The regularization parameter was set to $\tau = 10$ and the parameter β for balancing of horizontal to vertical smoothing was set to 1 (for details of the inversion algorithm see Section 4.3.1.3). The main difference to the original model is that the main anomaly is now clearly confined to the crust. Note that the volcanic arc is *not* underlain by high conductivity.

The high-conductivity zone leads to severe attenuation of electromagnetic fields which aggravates the resolution of deeper structures, particularly in the upper mantle and a possible root of the crustal anomaly. For the original model (Brasse et al. 2002) Schwalenberg et al. (2002) carried out a sensitivity analysis showing that the deeper parts of conductive structures are not resolved. In the forearc other crustal anomalies linked to arc-parallel but also arc-perpendicular faults blur the conductivity image at depth. It was thus a major aim to verify the lateral extent of the crustal conductor (i.e., may it be seen as a characteristic feature of the entire plateau?)

and to prove if the subduction-related fluid/melt cycle may be resolved in an alternative location of the high Andes.

4.3.1.2 The Central Altiplano

This study area is situated in the Bolivian Orocline or “Arica Bend” (named after the coastal town of Arica) at about 18°S, where the coastline and the structural trends change from N-S to NW-SE. Morphological segments of the forearc parallel to the trench correspond to an ancient magmatic arc which shifted eastward through time, recordable since the Jurassic (Scheuber et al. 1994) in the Coastal Cordillera, afterwards in the Longitudinal Depression, the Precordillera and until recently in the Western Cordillera. The forearc is incised by deep, E-W running valleys which open to the ocean; some of them may be associated with active faults. A system of west-vergent, steeply dipping thrust faults in the Precordillera is thought to be the location where the plateau was uplifted (Muñoz and Charrier 1996). The smooth monoclinic western flank of the plateau locally collapsed to form the giant Oxaya block (Wörner et al. 2002). Plio-Pleistocene to recent andesitic to rhyodacitic stratovolcanoes of the Western Cordillera are built on thick layers of ignimbrites which are widespread across the forearc until the coast and are dated between 22 and 19 Ma (Oxaya Ignimbrites) and 2.7 Ma (Lauca-Pérez Ignimbrite) (Wörner et al. 2000). Volcanic activity is less than to the south,

where the lithosphere is ~ 50 km thinner (Whitman et al. 1996); however, volcanoes are categorized from dormant (Parinacota) to solfataras state (Guallatiri) (González-Ferrán 1994), with ongoing activity probably reflected by shallow seismicity beneath the arc (Comte et al. 1999).

The most prominent structure of the Altiplano is the 80 km wide Corque Syncline where Tertiary strata reach a thickness of up to 10 km (Hérail et al. 1997). To the west the basin is bordered by the San Andrés-Villa Flor Fault which corresponds to the eastern limit of the Arequipa block, part of the Arequipa-Antofalla Massif with up to 2 Ga old rocks which underpins the Western Cordillera probably along the whole plateau (James and Sacks 1999), whereas to the east the basin is controlled by the Chuquichambi thrust system. The Coniri-Laurani Fault System marks the transition to the Eastern Cordillera, the rough eastern flank of the plateau, where rocks up to Ordovician age are exposed. Farther to the east the Main Andean Thrust and the Subandean in the Andean foreland present its actual deformation front with thin-skinned folding and thrusting, and large shortening rates (Allmendinger et al. 1997).

The MT profile extends from the Longitudinal Depression over the Precordillera, the Western Cordillera and the central Altiplano basin to the Eastern Cordillera, following a general trend of $N48^\circ E$ and thus roughly perpendicular to the main structural units and the contours of the Wadati-Benioff zone.

Data at 30 locations with a separation of ~ 10 km were collected during campaigns in late 2002 (Bolivia) and late 2004 (Chile, with a reference site in Bolivia occupied during both field studies). Several gaps in profile coverage were due to steep topographic gradients at the Western Cordillera Escarpment and in the Eastern Cordillera. Time series were processed by employing a robust, remote-reference code (Egbert 1997), yielding mostly stable and high-quality estimates of impedances and tippers in a period range from 10s–10000s. We may furthermore safely assume that the equatorial electrojet (EEJ) does not pose a problem as an inhomogeneous source in the investigation area according to an analysis of day/night time events (Friedel 1997) for data collected approx. 150 km farther south. The study presented here goes beyond a previous MT investigation on the central Altiplano (Ritz 1991) both by employing longer periods and by usage of magnetic field transfer functions.

Figure 4.7 exemplarily displays the real part of induction arrows along the profile for periods of 186 s and 1311 s. As mentioned above they should point away from good conductors in a two-dimensional setting. Remarkably, this is not the case in the forearc near the highly conductive Pacific Ocean (with a conductance of up to 25 000 Siemens at the trench); obviously conductive features running obliquely to the coastline (faults in the Coastal Cordillera?) deviate the direction of arrows to even coast-parallel. In the Precordillera,

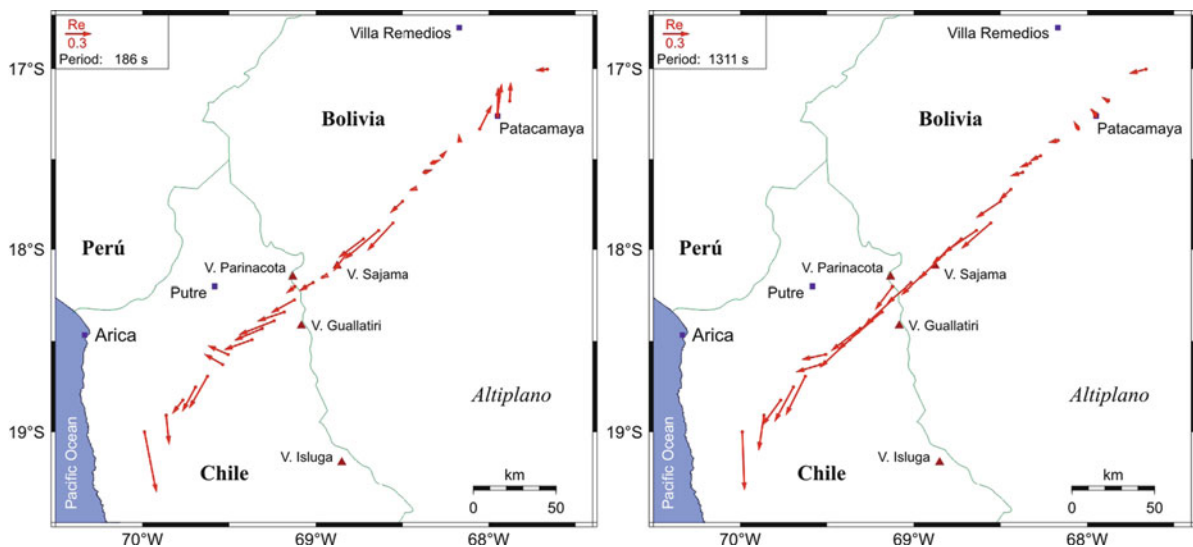


Fig. 4.7 Induction vectors for the Northern Altiplano at $T = 186$ s and 1311 s

the west-vergent thrust system and perpendicularly striking faults further complicate the situation. This is particularly obvious at the two sites near the Western Cordillera Escarpment and on the Oxaya Ignimbrites (*tic* and *oxa*). It shall be noted here that this deflection of arrow direction is observed in many other coastal and forearc parts of Chile as well (e.g., Brasse et al. 2009, Soyer 2002, Lezaeta 2001; see also below). In the volcanic arc and on the Altiplano proper, however, arrows at long periods point consistently parallel to the profile, indicating a strike direction of roughly NW-SE and thus parallel to main structural units. This is analogous to the situation farther south on the ANCORP profile (Brasse et al. 2002).

From the behavior of arrows several conclusions can be drawn immediately: (1) A 2-D interpretation is only meaningful for data on the plateau; the fore-arc data are clearly 3-D and thus discarded here for the time being. (2) Induction arrows at short periods show the margin of the well-conducting sediments of the central Altiplano basin. Unlike the south-western margin, the basement contact is not perpendicular to the profile near Patacamaya observatory. (3) The length

of arrows at long periods is still large in the volcanic arc and decreases to almost zero only on the central plateau; this indicates that a deep high-conductivity anomaly is not situated below the volcanoes but rather beneath the central Altiplano. (4) At the northeastern end of the profile long-period induction vectors do not reverse direction as would be expected if they were caused by a single deep anomaly below the Altiplano. This hints at an additional anomaly below the Eastern Cordillera.

This crude image of electrical conductivity distribution is also supported by analysis of impedances. Figure 4.8 displays characteristic transfer functions for the Precordillera, volcanic arc, Altiplano and Eastern Cordillera. *Forearc*: The coast effect predominates (large splitting of app. resistivities ρ_a and phases ϕ for xy- and yx-components), but note that the induction arrows do not point W-E. *Volcanic arc*: The coast effect becomes smaller, induction arrows are large and point away from a conductive structure farther to the east. *Altiplano*: App. resistivities in the Corque basin are generally very small, resembling a three-layer case, and induction arrows are almost zero

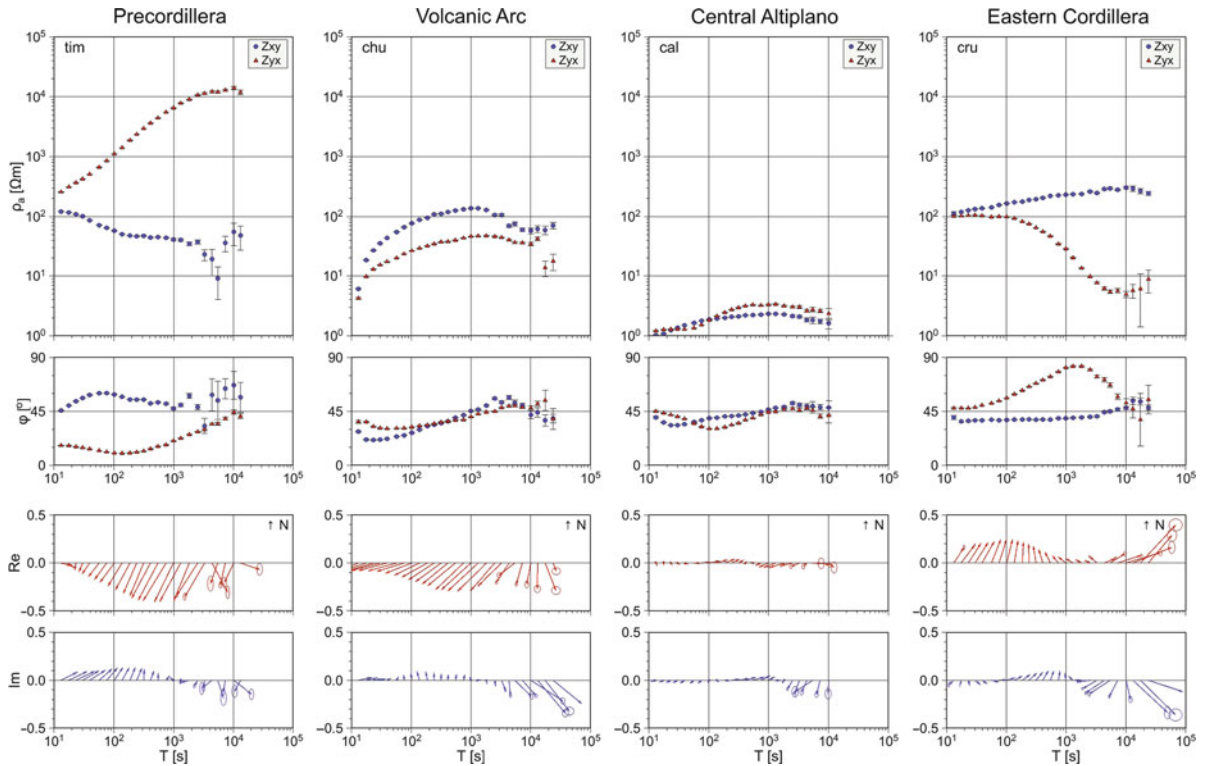


Fig. 4.8 Characteristic apparent resistivities, phases and induction vectors in the 4 morphological units crossed by profile A

indicating a conductive body at larger depth directly below. *Eastern Cordillera*: App. resistivities are higher again and strong splitting of ρ_a and ϕ is observed. Large, roughly northward pointing induction arrows at short periods indicate an additional conductivity contrast below the easternmost stations (*cru* and *lur*) or farther to the south.

A dimensionality analysis by calculating the skewness of impedance tensors reveals strong 3-D effects in the forearc while the rest of data may be regarded as 2-D: phase-sensitive skew values (being less prone to static effects) are below 0.3 – but note that this has to be regarded as a soft measure only; for definitions see, e.g., Bahr (1988). A notable exception is site *pat* (near Patacamaya geomagnetic observatory and the Coniri-Laurani Fault), where yx-phases leave the third quadrant reaching 45° at 20,000 s, an effect which may be explained by superposition of two anomalies with different strike directions at different depths and current channeling around a basement tip, extending into the highly-conducting sediments. Rotating these data into the coordinate system of regional strike (see below) yields normal phases in the first and third quadrant.

Decomposing the impedance tensor using a multi-site, multi-frequency scheme of McNeice and Jones (2001) provides estimates of regional strike for the whole profile as well as for single sites. According to the above mentioned 3-D influences, we first investigated the strike per station, which reflects again, besides the ocean effect at near-coastal sites, strong EW distorting influences at forearc stations. Thus excluding the forearc stations up to the western foothills of the high plateau provides quite a good fit for an unique strike direction of about $N40^\circ W$, approx. perpendicular to the profile direction. This single-site strike (arithmetically averaged over profile) is more or less consistent with the results of the multi-site, multi-frequency routine, which yields $N38^\circ W$ strike direction for the plateau stations. Taking into account the average magnetic declination of approx. $N4^\circ W$ (MT fields are usually measured in geomagnetic coordinates), this strike is indeed almost exactly perpendicular to the profile direction ($N48^\circ E$). Note, however, that this coincidence is fortunate: there is only a single accessible road along which sites could be deployed.

4.3.1.3 2-D Model Finding and Interpretation

With the arguments given above we assumed a common electrical strike of $N38^\circ W$ for all plateau sites and rotated all data by -38° into profile direction. Since strong 3-D effects do not permit 2-D modeling of forearc sites, they were discarded from further analysis as presented below. A qualitative explanation of coast-parallel induction arrows can be achieved by assuming structural anisotropy in the upper forearc crust, as was already shown for South Chilean data Brasse et al. (2009) by employing the anisotropic 2-D forward algorithm of Li (2002).

A basic model (Brasse and Eydam 2008) incorporates the Pacific Ocean with crude bathymetry, a highly-resistive forearc with an embedded anisotropic layer between $z = 5$ and 20 km and a strike direction of the conductive axis of $N20^\circ W$, simulating a deeply fractured crust in accordance with the strike of the Precordillera Fault System in this area. At the margin of the anisotropic layer and without the ocean present, large induction arrows have a $N110^\circ W$ direction, perpendicular to the conductive axis. The coupling of the ocean and the anisotropic layer leads to a dramatic deflection of induction arrows from the expected W-E direction if only the coast effect would be present. For further explanation of the effects occurring at an anisotropic continental margin see the more systematic study of Brasse et al. (2009). A more quantitative investigation would have to take the true bathymetry into account as well as local structures in the forearc. This – or an equivalent full 3-D approach – goes far beyond the scope of this manuscript and is not followed for the time being.

Not taking into account the forearc stations has another positive consequence: the coast effect is much smaller for sites on the plateau (from the closest site *cat* distance to the coast is 90 km, to the trench 230 km) and important for very long periods only; it thus suffices to incorporate bathymetry in a crude manner. Nevertheless, the influence of the ocean is perhaps not purely 2-D due to bending of the trench near Arica; this has possibly to be considered in interpretation (Eydam 2008).

As in most of the modeling examples in this text, we employed the non-linear, conjugate gradient algorithm of Rodi and Mackie (2001) to carry out the 2-D inversions. It is based on a Tikhonov-type regularization by minimizing the objective function

$$S(\mathbf{m}) = \|W_d(\mathbf{d} - F(\mathbf{m}))\|^2 + \tau \|W_m(\mathbf{m} - \mathbf{m}_0)\|^2 \quad (4.10)$$

with \mathbf{d} denoting the data vector, \mathbf{m} the model vector, t the transpose, W_d a data weight matrix (usually the data variances) and τ the regularization parameter. $F(\mathbf{m})$ is the model response, \mathbf{m}_0 the starting or an *a priori* model, $\|\dots\|$ the norm, and W_m the regularization operator, often set as the Laplacian $(\nabla^2 \mathbf{m})^2$. W_m incorporates a weighting function $w(x,z)$ allowing to penalize horizontal or vertical exaggeration of model structures (R. Mackie, 2-D inversion manual):

$$\mathbf{m}^t W_m^t W_m \mathbf{m} \approx \int w(x,z) (\nabla^2 \mathbf{m})^2 dA; \quad (4.11)$$

integration is over model area A . If an uniform grid is chosen for W_m , then

$$w(z) = (z(k)/z_0)^\beta \text{ for } z(k) > z_0 \text{ and} \quad (4.12)$$

$$w(z) = 1 \text{ for } z(k) \leq z_0 \quad (4.13)$$

where $z(k)$ is the thickness of the k -th row and z_0 the minimum block thickness, which has to be set manually.

The misfit between data and model response is calculated as a root mean square error according to:

$$rms = \sqrt{\frac{(\mathbf{d} - F(\mathbf{m}))^t W_d^{-1} (\mathbf{d} - F(\mathbf{m}))}{N}} \quad (4.14)$$

with N = number of data points. Under practical conditions, W_d contains only the main diagonal, i.e., the data variances. Note that this misfit measure depends on the data errors and care must be taken if analyzing a model fit by looking at the rms alone; this is particularly important if an error floor is set.

Numerous experiments have to be conducted to achieve a best-fitting and reliable final model. Although these tests should be a standard procedure in non-linear, regularized inversion, they are briefly mentioned here: (1) variation of the starting model and influence of the ocean; (2) exploration of model space by varying the regularization parameter yielding a trade-off curve (ideally L-shaped) between rms fit (root mean square) and model roughness (e.g., Asters et al. 2005); (3) assigning specific error floors to individual

components, i.e., TE and TM mode (from tangential-electric and -magnetic, referring to the field parallel to conductivity contrasts) resistivities and phases, and tippers, as well as checking for static effects; (4) sensitivity tests and tests of (in)significant model features; (5) discretization; (6) convergence and number of iterations. Another important aspect is to check individual components separately: Due to different boundary conditions at interfaces, TE and TM mode impedances and tippers are sensitive to different subsurface structures.

Topographic effects play only a minor role along the profile with the exception of sites *par* (at the foot of Parinacota volcano) and *lur* in a river valley of the Eastern Cordillera. This may at first glance be surprising considering the high altitude of the study area, but the Altiplano is a vast plain with low intermittent ranges. Even in the volcanic arc, wide and only marginally undulating plains dominate the landscape between the individual volcanic edifices, making the terrain ideally suited for magnetotelluric work. Test modeling shows that at long periods >10 s the topographic effect reduces to a static shift problem (for 2-D only in TM mode) which is treated in the inversion process described above.

For the resulting model (Fig. 4.9), obtained by jointly inverting tippers, TE and TM mode apparent resistivities and phases, we chose a regularization parameter of $\tau = 10$ which lies in the corner of the trade-off curve (but note that the L-shape is not well expressed (Eydam 2008)). Error floors were set to 20% for apparent resistivities and 5 % ($\approx 1.45^\circ$ absolute) for phases, thus assigning a higher weight to phases in order to overcome the static shift problem. This procedure leads to app. resistivity curves shifted with respect to the data, while the phases are usually fitted well. Of course, the mentioned parameters are only for the data under consideration, other data sets may require different settings. The statics issue was further addressed by inverting for shift factors with the underlying (and perhaps not always unproblematic) assumption that the product of these factors should be one along the profile. Static shift in TM mode data is treated easily in a 2-D model by setting a small cell beneath a station to an adequate value; it may, however, be misleading in the case of TE mode. Here the shift results from inhomogeneities perpendicular to the profile (i.e., 3-D structures) and correcting this may require a change of structure at depth in the 2-D model (which is thus

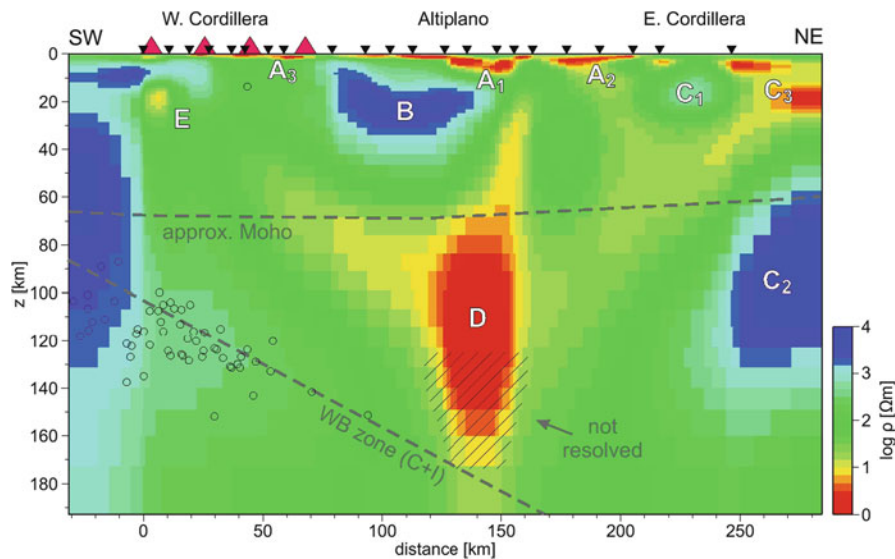


Fig. 4.9 Resistivity model for the central Altiplano in Bolivia and northernmost Chile (Brasse and Eydam 2008)

not a real static problem any more; shifts at neighboring sites may also be contradictory). Therefore some investigators prefer not to use TE mode at all or restrict themselves to TE phases only (see, e.g., Wannamaker et al. 1989).

Since tipper data are very consistent on the Altiplano, their weight was set very high with respect to impedance-derived data by assigning a small (absolute) error floor of 0.02. At site tak only tipper data could be used due to layout problems with the telluric lines. The general features of the model are not changed if the error floor for apparent resistivities is set higher, e.g., to 100 %. The resulting rms of the model displayed in Fig. 4.9 is 1.64, data fit is exemplarily shown for periods of 186 s and 1311 s along the profile in Fig. 4.10 and as pseudo sections in Brasse and Eydam (2008).

The “final” inversion model shows that the whole Altiplano crust and even the upper mantle are generally characterized by relatively low resistivities in the range of 100 Ωm , surrounded by high-resistivity zones at the SW and NE margins. Several structures which are consistently resolved throughout the inversion runs can additionally be identified (marked by letters in Fig. 4.9):

(A) The up to ~10 km thick Tertiary sedimentary layers of the central plateau, particularly in the Corque Syncline (A_1), are well resolved. The asymmetric geometry of the conductive layer fits

well with the reconstruction of geological history for the region (Hérail et al. 1997, Sempere et al. 1990) and the prior study of Ritz et al. (1991). The eastern limit of the Corque Syncline is defined by the Chuquichambi thrust system (seen as an interruption of the low resistivities at sites *cal* to *rio*), marking a transition to another, less deep sedimentary basin to the east, a northern extension of the Poopó Basin (A_2) (Hérail et al. 1997). The very low resistivities of approx. 2 Ωm are most likely due to saline fluids which in turn may stem from buried salars (salt pans) – while salars are not exposed at the surface in the actual study area, they are a characteristic feature of the southern Altiplano. A_3 depicts the sediments between Parinacota and Sajama volcanoes; on the other hand the intra-arc Lauca Basin at the southwestern margin is either not very conductive or does perhaps not reach deep enough for the period range considered here to be characterized by low resistivities.

(B) An upper to middle crustal (up to 25 km depth) zone of high resistivities (>1000 Ωm) extends between the arc and the Corque Basin. Its north-eastern margin coincides with the superficial trace of the San Andrés Fault which is also marked by a strong contrast in seismic velocities separating the relatively fast volcanic western Altiplano from the slow sedimentary basin to the east (Dorbath

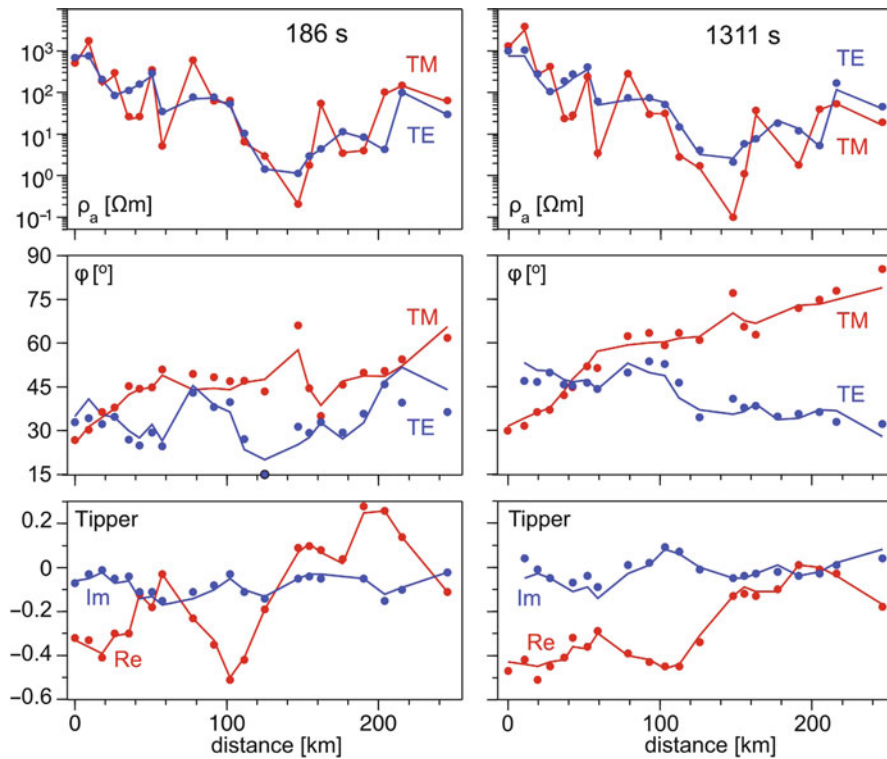


Fig. 4.10 Data and model response for 2 periods along the profile (Brasse and Eydam 2008)

and Granet 1996). This resistive, fast and thus rheologically strong structure may be correlated with old cratonic crust of the Arequipa block (see introduction).

- (C) Passing the Coniri-Laurani Fault Zone to the east (sites *cru* and *lur*) higher resistivities (C_1) probably indicate the transition to the crystalline (Paleozoic) basement of the Eastern Cordillera. At larger depths the Eastern Cordillera is imaged as a very bad conductor (C_2), again in accordance with very high seismic velocities deduced by (Dorbath and Granet 1996). Interestingly, a good conductor (C_3) appears here at mid-crustal depths; this conductor was already mentioned in the section on data description and may well correlate with the conductivity anomaly running along the Eastern Cordillera, proposed by (Schmucker et al. 1966). Note, however, that this structure is at the margin of our study area and thus not well resolved.
- (D) The most obvious anomaly is, however, located in the upper mantle and reaching into the lower crust below the central Altiplano, where resistivities are as low as 1 Ωm . This conductor would be in good

accordance with the “standard model” of subduction (partially molten asthenospheric wedge) if its location were not 80-100 km northeast of the recent volcanic arc, i.e., already in the backarc (see discussion below).

- (E) At the southwestern end of the profile, below the margin of the volcanic arc, a modest conductor is visible at mid-crustal depths. Although it may indicate a deep magma chamber, it should be noted that there is no recent volcanic activity observable at the surface; dormant Taapaca volcano is located 50 km farther to the NW. Due to its location at the edge of the profile and the increasing three-dimensionality in the adjacent forearc, this structure is poorly resolved.

Resolution analysis encompassed visualization of the sensitivity matrix and tests for significant structures by modifying their resistivity and/or geometrical borders. The highest sensitivity values are observed for the sedimentary basins and the mantle conductor. The more marginal conductors have higher sensitivities compared with their surroundings, too, but note that these features are not as consistently modeled in

the different inversion runs as the basins and the mantle structure.

Several experiments to test resolution of the latter have been carried out, e.g., replacing the low resistivities with more normal values of 50 Ωm (leaving the other structures unchanged) worsens the rms from 1.64 to 4.94, an unacceptable increase of misfit. Then the inversion was started over, leading the conductor to appear again after a few iterations. The deeper parts (>120 km) on the other hand have only negligible influence on the model response and may thus be considered as unresolved (hatched area in Fig. 4.9). The principal features of the model in Fig. 4.9 did not change, if only a restricted period range (e.g., omitting all periods below 100 s) was used; the same statement holds for a variety of starting models. Another test concerned the location at depth: Can the measured data also be explained if the conductor is shifted entirely into the crust? As above, we replaced the low resistivities in the mantle with values of the surrounding mantle, placed a conductor in the mid-crust and started the inversion again. After 50 iterations the resulting rms is at an acceptable level of 1.85, but the conductor is moved deeper towards the Moho. The relatively good fit, however, is achieved at the cost of unrealistically low resistivities of 0.01 Ωm ; this alternative model is therefore discarded.

The individual inversions of TE, TM and tipper data (which all achieved an rms in the range from 1.1 to 1.4) showed that the mantle conductor is best resolved by the tipper and (with slightly lower conductivities) in TE mode; both data subsets are in general agreement. On the other hand TM mode senses only a broad and diffuse high-conductivity zone at lower crustal/upper mantle levels, which is expected: TM data are less sensitive to deep, dyke-like structures. For upper crustal features all 3 subsets agree reasonably well in accordance with the model in Fig. 4.9.

4.3.1.4 The Asthenospheric Wedge

While most of the conductive and resistive features displayed in Fig. 4.9 are easily explained and agree well with other geological and geophysical background information, the deep high-conductivity zone in the upper mantle below the central Altiplano poses problems regarding its high core conductivity and its unexpected location with perhaps far-reaching consequences. Although such an anomaly as an image of melts in the asthenospheric wedge above the subducted

plate is not surprising as such, it is not situated below the volcanic arc but rather shifted by 80–100 km toward the backarc. This does not seem to be unique for the Altiplano plateau: there are weak hints from profiles farther south at 21°S and 20.5°S that there exists a similar conductivity pattern off the volcanoes at large depths (e.g., Brasse et al. 2002, Schilling et al. 2006). On the southern Altiplano, however, this could not be resolved unambiguously due to lack of resolution below a huge crustal conductor. As Heit (2005) has shown the whole mid- and lower crust below the plateau at 21°S is also characterized by anomalously low seismic velocities, thus supporting the hypothesis of large volumes of partial melt in the mid- to lower crust. This large-scale conductor is missing below the central Altiplano (with the exception of near-surface conducting sediments), thus enabling insight into deeper segments of the subsoil.

An estimation of melt rates in the wedge may be achieved by assuming a simple two-phase system with near-perfect melt interconnectivity (Hashin-Shtrikman upper bound). The melt rate is critically dependent on conductivity of the melt phase (σ_m), which is in turn a function of temperature and composition. Melt composition for ultramafic material changes from nephelitic (above 2 GPa) through alkaline-basaltic to tholeiitic with increasing temperature or melt fraction, respectively (cf., Tyburczy and Fisler 1995, Roberts and Tyburczy 1999). In order to feed a volcanic arc, significant melting must occur in the wedge, which implies a minimum temperature of $\sim 1300^\circ\text{C}$ (Schmidt and Poli 1998). Conductivity σ_s of the solid phase is comparatively unimportant; as function of temperature for dry, semi-conducting rocks it follows an Arrhenius law, and we may assume a σ_s in the order of 0.01–0.005 S/m at upper mantle depths.

The modeled bulk conductivity inside the wedge core is in the order of 1 S/m (Fig. 4.9), similar to the crustal conductor below the ANCORP profile and about an order of magnitude larger than the high-conductivity zones in South Chile (Brasse and Soyer 2001). For a basaltic to tholeiitic melt composition at 1300°C, we may assume a melt conductivity of $\sigma_m = 5.5 - 6.5$ S/m, resulting in a melt fraction estimate of 21–25 vol.%.

This value is very high, but note that conductivities are for dry magmas which are less frequent in subduction zones. Subduction zone magmas contain at least 2–3 wt% water in the hot core of the mantle

wedge Gaetani and Grove (2003); water content may even increase to 30 wt% for first magmas near the slab according to Grove et al. (2006). The supply of water enhances the melt conductivity considerably (Gaillard 2004); additionally higher temperatures or saline brines may further increase conductivity and thus reduce melt rate. For instance, a hotter wedge (1 400°C) implies a σ_m of 11.5 S/m for tholeiitic melt, yielding a value of 12.5 vol.%.

Conductivities of mantle fluids are difficult to assess. Deep crustal fluids are known to reach very high conductivities of up to 100 S/m (Nesbitt 1993), depending on their ionic composition. For slab-derived mantle fluids one may assume similar values based on high salinities found in fluid inclusions (Scambelluri and Philippot 2001). The input of saline fluids into the hot wedge may thus significantly reduce the bulk resistivities, yielding a melt rate in the order of 5 vol.%. In general the high melt rates estimated from electrical conductivities are principally in accordance with new geochemical results (Grove et al. 2006), revealing that the amount of hydrous melt may reach values of 10–15 wt.%.

Very recently, Gaillard et al. (2008) presented laboratory measurements of carbonatite melts with their conductivity values exceeding the numbers mentioned above by more than an order of magnitude. If such melts would be present in the Central Andes, they would reduce the necessary melt fraction significantly. However, such an occurrence is not documented to the author's knowledge.

To understand the location of the highly conductive part of the wedge, Fig. 4.9 also displays the projected locations of earthquakes (lying within a lateral distance of 50 km from the profile), extracted from the catalogue of Engdahl and Villaseñor (2002). As expected hypocenters are clustered below the volcanic arc at depths of 100–130 km (with an additional, single event in the crust below the volcanoes at the Chilean-Bolivian border). Major earthquake activity ceases at depths >150 km (leaving apart the very deep events below the eastern Andean foreland), still far from the anomaly, which is located above a slab depth of 160–200 km. The catalog only comprises larger events ($M > 4.5$), but there is no indication of smaller events according to the local tomography study of Dörmann and Granet (1996); this may, however, be a problem of resolution.

Attenuation data for the mantle below the central Altiplano are scarce. The images given by Baumont

et al. (1999) and Myers et al. (1998) touch our study area only marginally and refer mainly to the crust; however, their conclusion about a heterogeneous and generally highly absorbing crust is in accordance with the conductivity image. The best correlation exists perhaps with an upper mantle high attenuation (low Q) zone (Myers et al. 1998) and low v_p velocities (Dörmann and Masson 2000) at 19.5°S. The well-conducting asthenospheric wedge is also in accordance with low densities in the uppermost mantle in the 3-D model of Tassara et al. (2006), explaining – together with the thickened crust – the large Bouguer anomaly of –400 mGal (locally –450 mGal) on the plateau.

There is an interesting correlation between our deep Altiplano model and the seismic attenuation model of Schurr et al. (2003) for the Puna plateau at about 24–25°S. It proposes vertical as well as non-vertical rise of fluids/melts in the backarc and fluid release from the downgoing slab at similar depths as the MT model presented here. The situation in the Puna, however, differs somewhat with respect to a zone of major seismicity in the backarc, directly below the anomaly. Due to the unfavorable distribution of earthquakes below the Andes at 18°S, a highly attenuating wedge corresponding to the resistivity model would be difficult to detect (i.e., only far to the east, perhaps beyond the Eastern Cordillera).

Intermediate-depth earthquakes are commonly understood as consequences of fluid release from the subducted slab (dehydration embrittlement, e.g., Kirby et al. 1996, Hacker et al. 2003). Due to propagation of hydraulic fractures rise of fluids into the overlying mantle is not vertical according to Davies et al. (1999). Corner flow may additionally transport the fluids farther away from the source region, including subsequent hydration and dehydration, perhaps in addition to a mechanism described by Mibe et al. (1999). Dependent on P-T conditions the released fluids may not form an interconnected network directly at the source (dihedral angle Θ above 60°); the hydrous peridotite (with fluids in isolated pockets) is dragged downward until an open network ($\Theta < 60^\circ$) may form, e.g., at 1 000°C and 4 GPa.

A massive influx of fluids into the continental mantle may be facilitated by an increase of slab dip as was proposed for areas farther south (e.g., Kay and Mpodozis 2001); a larger subduction angle compared to the general Cahill & Isacks image of Wadati-Benioff contours has recently been deduced from local earthquake tomography by (David 2007) for the orocline,

too. We can of course not exclude the scenario, but in this case one would assume the highly conductive wedge farther to the west.

From the asthenospheric wedge melt rises upwards, perhaps being stored in a MASH zone (melting, assimilation, storage, and homogenization) at the crust/mantle interface according to Hildreth and Moorbath (1988) before rising further into the crust, imaged by rather low resistivities in the MT model. The highly resistive Arequipa block seems to force a bifurcation; one branch leads subvertically to the central Altiplano. There are indications for another, non-vertical rise, too: From the upper part of the conductor a pathway with intermediate resistivities (20–60 Ωm) may be identified, passing obliquely through the crust until below the Western Cordillera volcanoes. Note that there is no indication of recent volcanic activity on the central plateau, perhaps with the exception of Cerro Colluma, a maar SE of the profile which may have been active in the Holocene (Smithsonian Global Volcanism Program, volcano no. 1505-024). But it should also be noted that heat flow on the plateau is widely enhanced – in the order of 100–120 mW/m^2 (e.g., Springer and Förster 1998, Hamza and Muñoz 1996) – and, although reliable data are sparse and scattered, likely higher than in the volcanic arc itself. One may perhaps speculate that we are observing the formation of a new volcanic arc and thus a momentary view of its eastward migration, as it has occurred already several times since the Jurassic.

The Altiplano plateau has been subject to extension during its initial build-up phases; if this tectonic pattern would be persisting until today, it would be difficult to explain why the partial melts would not reach

the surface. Since about 18 Ma, however, shortening – i.e., compression – is observed on the entire plateau (Scheuber et al. 2006).

Individual volcanoes and possible magma chambers or conduits have not been the target of this study. To achieve a detailed conductivity image at upper crustal depths below the edifices a far denser data sampling including higher frequencies would have been necessary. Due to their enormous height (Parinacota 6348 m, Sajama 6542 m a.s.l.) a well-suited network of sites is difficult to construct.

Fluid release in and above the subducting slab further trench-ward has not been modeled along this profile, and including these as a-priori, well-conducting features did not prove to be successful; they were converted to highly resistive during the inversion process. As stated above, the conductivity image in the forearc is overprinted by 3-D crustal anomalies, and the part of the profile which is interpretable in a 2-D approach is too short to resolve a low-resistivity zone above the slab unambiguously.

The dominance of the backarc in the conductivity image is also emphasized in a further model more to the south at $\approx 24^\circ$ S. Profile C extends from the Precordillera, crosses the Salar de Atacama and the Western Cordillera (S of highly-active Lascar volcano) and end for the time being in the western Puna plateau. Again the volcanic arc is not conductive (except near Lascar itself, where a HCZ is modeled south of the edifice Diaz (2010)), but beneath the Puna appears a huge conductor (Fig. 4.11). Its eastern and lower extensions can't be resolved due to the current lack of stations in Argentina, but there is striking correlation with seismic tomography (Schurr et al. 2003).

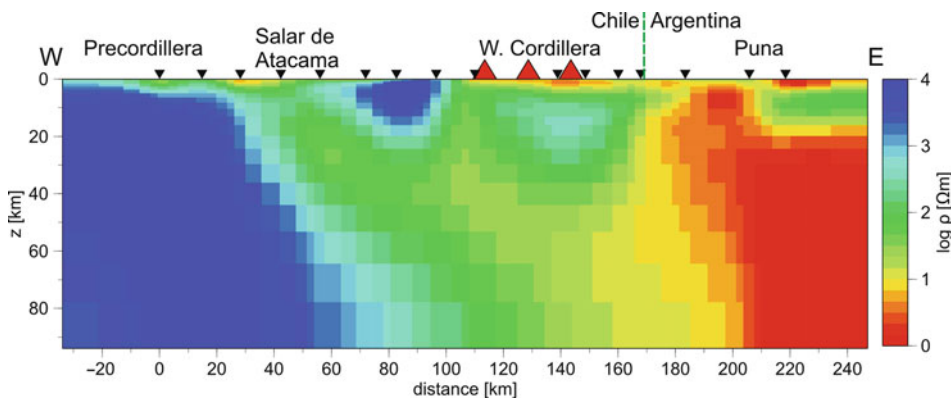


Fig. 4.11 Resistivity model for profile C

4.3.1.5 Conclusion for the Central Andes

New deep electromagnetic sounding data from the Bolivian orocline in the central Andes have been collected. They may be analyzed with a two-dimensional approach for the high plateau, but strong 3-D effects prevail in the Chilean forearc. Here data are tentatively explained by 2-D models incorporating structural anisotropy in the crust with a preference direction of electrical conductivity parallel to the strike of a prominent forearc thrust fault system. Classical 2-D modeling is thus restricted to the plateau, including the volcanic arc, the Altiplano basin and the margin of the Eastern cordillera. Strike directions deduced from impedance data agree well with those obtained from tipper data at long periods.

The 2-D inversion revealed several high-conductivity and high-resistivity zones in the crust and upper mantle of the central Andes. They are interpreted as images of sedimentary basins of the central Altiplano plateau, still uncertain (due to lack of resolution), partially molten regions below the Western Cordillera and the consolidated Precambrian Arequipa block, respectively. The main result is the image of the conductive asthenospheric wedge and a conductor rising into mid-crustal levels. This large anomaly is located already in the backarc, i.e., not beneath the current volcanoes. This may imply that we observe a snap-shot of the migration of the arc, as it has occurred frequently since formation of the subduction system.

On the other hand, no large-scale conductor in the crust as in the Southern Altiplano has been detected, which is thus not a characteristic feature of the entire plateau as was presumed earlier. To understand and incorporate transfer functions in the forearc, more complete approaches than the 2-D modeling investigations presented here are necessary, particularly near the coast and at the western margin of the plateau. This includes additional, denser data sampling in Northern Chile and extension toward 3-D modeling, forming the task for future work.

4.3.2 The Southern Andes

In South-Central Chile between latitudes 38°S and 41°S (Fig. 4.12) the oceanic Nazca plate is subducted beneath the South American continent and the great

earthquake of 22 May 1960 (moment magnitude $M_w = 9.5$) initiated (Cifuentes 1989). Subduction is oblique with an angle of $\sim 25^\circ$ (i.e., N77°E) with respect to the plate margin and with a current velocity of ~ 6.5 cm/a (Klotz et al. 2006). The study area is located in the northernmost Patagonian (Neuquén) Andes and can be subdivided into several main morphotectonic units (e.g., Folguera et al. 2006, Melnick et al. 2006): (1) a narrow Coastal Platform comprising uplifted Tertiary marine and coastal sequences; (2) the Coastal Cordillera, formed by a Permo-Triassic accretionary complex and a late Paleozoic magmatic arc; (3) the Longitudinal Valley, a basin filled with Oligocene-Miocene sedimentary and volcanic rocks, covered by Pliocene-Quaternary sediments; (4) the Main Cordillera, formed by the modern magmatic arc and intra-arc volcano-sedimentary basins; (5) the Loncopué Trough, already in Argentina, an extensional basin east of the Main Cordillera associated with abundant mafic volcanism; (6) the southern extension of the Agrio fold-and-thrust belt; and (7) the Mesozoic Neuquén Basin and the Cretaceous-Tertiary foreland basin to the east.

Subduction at the Chilean margin started already in the late Paleozoic, while Andean evolution began in the Jurassic, associated with the opening of the South Atlantic Ocean. In the Cretaceous widespread plutonism occurred in the Coastal Cordillera and in the area of the volcanic arc, where the Patagonian Batholith was formed. South of 38°S the position of the volcanic arc remained relatively constant through time with the exception of a significant broadening of the magmatic system (Muñoz et al. 2000) and an 80–100 km westward shift of the volcanic front in the late Oligocene-early Miocene with respect to its current position (Parada et al. 2007). This event was probably related to the breakup of the Farallon plate into Nazca and Cocos plates, respectively, and subsequent changes in plate convergence and subduction angle (Muñoz et al. 2000). For further description of the tectonic evolution see the overview articles by Stern (2004), Ramos and Kay (2006), and Glodny (2006).

The modern Principal Cordillera is dominated by the Holocene volcanoes of the Southern Andean Volcanic Zone, with some of the most active volcanoes in South America, e.g., Villarrica, Llaima and Lonquimay (González-Ferrán 1994). The chain of

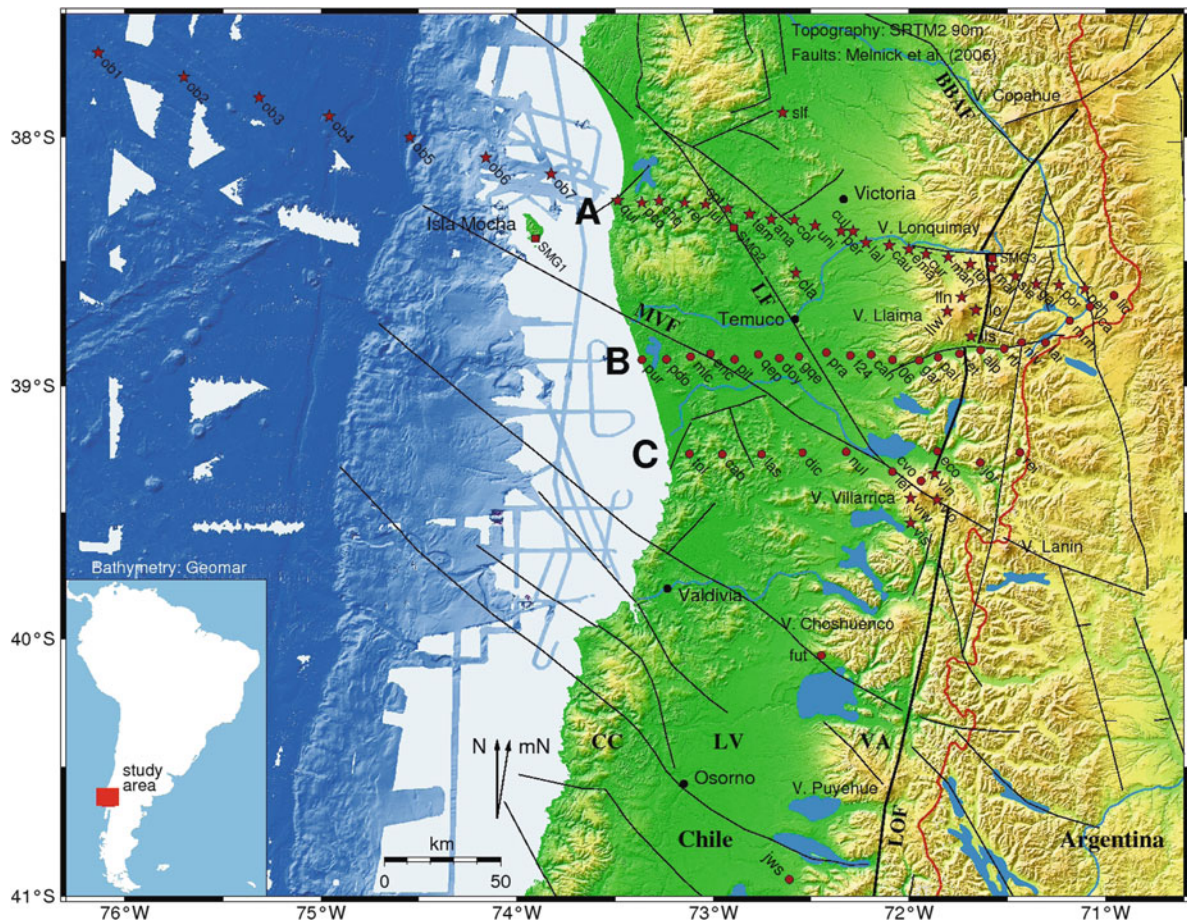


Fig. 4.12 Magnetotelluric sites in Southern Chile. Topography is based on SRTM data, while swath bathymetry was obtained aboard RV Sonne during various cruises (Scherwath et al. 2006)

stratovolcanoes is aligned parallel to the trench and along the Liquiñe-Ofqui Fault (LOF), a mega shear zone extending for over 1 000 km from the triple junction of Antarctic, South American and Nazca plates to $\sim 38^\circ\text{S}$ (Cembrano et al. 1996, 2007). A NW-SE – thus obliquely to the trench – oriented fault system crosses the arc and forearc, e.g., Melnick et al. (2006), which may have been of importance for a major eruption in the Cordon Caulle volcanic complex immediately after the $M_w = 9.5$ earthquake (Lara et al. 2004). The Lanahue Fault, in particular, is regarded as an inherited, continuously reactivated, pre-Andean structure, which is associated with deep-reaching seismicity (Yuan et al. 2006).

Two long-period magnetotelluric campaigns were conducted, an earlier one in 2000 and an additional field experiment in austral summer 2004/2005, which also included an amphibious component

employing sea-bottom instruments from Woods Hole Oceanographic Institution (WHOI). While the first experiment (Brasse and Soyer 2001, Soyer 2002) was carried out in the framework of the multi-disciplinary programme SFB 267 “Deformation Processes in the Andes”, the second one (Kapinos 2011) was part of the TIPTEQ project (“From the Incoming Plate to Megathrust Earthquakes”), with other subprojects dealing with passive and active seismology, gravity and geology/tectonics. Structural information at the South Chilean margin in the study area concerning Moho depths and geometry of the downgoing plate may particularly be inferred from a large number of recent seismic experiments (Bohm et al. 2002, Lüth and Wigger 2003, Rietbrock et al. 2005, Haberland et al. 2006, Krawczyk et al. 2006).

During the two campaigns, a total of 72 stations were deployed between the Argentinian border and

the Pacific Ocean, yielding electromagnetic (MT and GDS) transfer functions in the period range between 10 s – 20,000 s. On land, the network encompasses the areas of the Coastal Cordillera, the Central Depression or Longitudinal Valley and the Principal Cordillera (see Fig. 4.12). The seafloor stations (from Woods Hole Oceanographic Institution) were deployed across the Peru-Chile trench during RV Sonne cruise SO181. Since analysis of offshore sites is not completed yet, we restrict the following study to the onshore component of the experiment.

4.3.2.1 2-D Modeling – The Standard Isotropic Approach

An early modeling approach by inverting only impedance data was carried out (Brasse and Soyer 2001) for the central profile at 38.9°S in Fig. 4.12, which corresponds to the seismic ISSA line (Lüth and Wigger 2003). The major result was the detection of a good conductor beneath the Central Valley, probably associated with the Lanalhue Fault (formerly known as Gastre FZ, obliquely traversing the northern Patagonian Andes in a SE-NW direction), and a high conductivity zone beneath the volcanic arc.

We extended this modeling study by incorporating tipper transfer functions and known a-priori information like highly accurate swath bathymetry data, obtained during several cruises of RV Sonne (Scherwath et al. 2006); the result is shown in Fig. 4.14. Another feature included in the starting model is a highly-resistive slab of the subducted Nazca Plate, an assumption justified by EM measurements on the seafloor (Chave et al. 1991). As in the previous model a common strike direction of 0° was assumed, justified by multi-site, multi-frequency analysis of strike directions according to Smith (1997) and the phase tensor plot in Fig. 4.13. Regularized inversion was carried out with the non-linear conjugate gradient code of Rodi and Mackie (2001); the regularization parameter was set to $\tau = 10$. Error floors were set to 20% for apparent resistivities, 5% for phases, and 0.1 (absolute value) for real and imaginary parts of the tipper. Since tipper data are not consistent with impedance strike directions (see below), we used their projection on the y-(EW)-axis. Further details concerning inversion settings and sensitivity issues, which reach beyond the purpose of the study presented here, are described by Kapinos (2011).

In terms of a root mean square error, the obtained data fit is remarkably good with a $\text{rms} = 1.1$; but note that this is mainly due to the relatively high error floor assigned to the tipper data. However, model structures do not change significantly if a different weighting of data relative to each other is applied (Kapinos 2011). Furthermore, the main structures are only marginally affected, if different starting models are used (e.g., a homogeneous half space with the Pacific Ocean included). Since isotropic modeling is not the main topic of the study presented here, we skip discussion of data fit and sensitivities here and just investigate the major features of the model.

As in Brasse and Soyer (2001) the main conductors (B, C and C' in Fig. 4.14) are located beneath the Central Valley and the volcanic front. The highly-conductive zone C at mid-crustal depths beneath the volcanic arc seems particularly interesting: The profile runs just south of Llaima volcano, and the model may simply image a large magma deposit beneath, but offset by ~10 km to the east. Note that Llaima erupted violently on 1 January 2008, but also note that these data were collected already in 2000, and it is of course not known how this eruption may have affected the conductor by removing or relocating a significant part of the magma deposit.

The Central Valley conductor on the other hand, beneath the trace of the Lanalhue Fault, is unlikely to originate from partial melts due to temperature considerations in the (relatively cold) forearc – fluids are seen here as the main cause of elevated conductivities. A consistent feature is conductor D east of the eastern margin of the profile (already in Argentina) – although not truly resolved with respect to location and resistivity due to the lack of stations, it appears in all inversion runs. A preliminary explanation may lie again in a root zone for the Holocene backarc volcanism in the Loncopué Trough. However, only a future extension of the profile into Argentina could unambiguously answer this question.

A very good conductor (A, not well visible on the southernmost profile) appears west of the transects already beneath the ocean, overlying the downgoing plate. This structure is not seen when only crude bathymetry is taken into account (Brasse and Soyer 2001) – this underlines the importance of exact bathymetry for near-coastal data. It may at first glance seem like an inversion artifact; however, it is also modeled at the northernmost TIPTEQ profile, where an

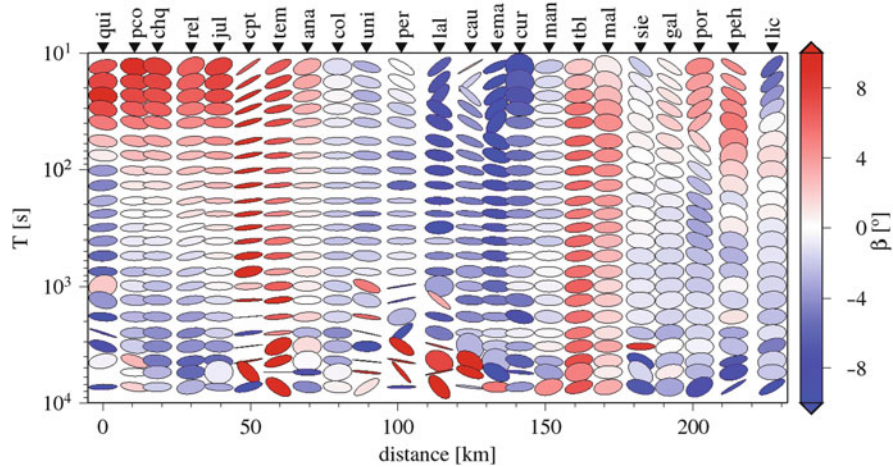


Fig. 4.13 Phase tensor ellipses for the northern profile A (Kapinos 2011)

additional offshore station was incorporated (Kapinos 2011). Furthermore, it correlates with a strong seismic reflector (Groß et al. 2007) beneath the TIPTEQ traverse. The origin of this structure remains enigmatic for the time being, but analysis of seismic tomography data suggests a possible low-velocity zone (Haberland, pers. comm.) and thus a fluid-rich accretionary wedge, perhaps fed by faults originating at the downgoing plate. Interestingly, the overall appearance of the model with its several conductors – particularly structure A off the coast – is quite similar to a model recently published by Soyer and Unsworth (2006) for the Cascadia subduction zone in SW Canada.

The subducted Nazca plate was modified in the course of the inversion process, leading to a much more heterogeneous image of the slab; additionally several poor conductors are now seen in the continental crust, rising from the plate interface. Apart from the main features in Fig. 4.14, minor structures also include the near-surface, but not-deep reaching sediments in the Central Valley in accordance with tectonic assumptions (H. Echtler, pers. comm.).

Although the 2-D inversion model appears like a plausible result particularly with respect to the resolved conductive features beneath the profile, it cannot represent a “true” model in an important aspect: its response only approximates the vertical magnetic field data, which are significantly and systematically distorted throughout the study area. Furthermore, the number of conductive “blobs” of the model, resembling the study of Heise and Pous (2001), suggest a different,

anisotropic approach. This is treated in the following sections.

4.3.2.2 GDS Transfer Functions in South-Central Chile

The Chile trench reaches a depth of $\sim 4\,600$ m in the study area, yielding a conductance of 14,000 S (Siemens); taking into account the – presumably well-conducting – sedimentary filling this value should even be higher. Tipper magnitude directly at the coast is $W \approx 0.8$ for long periods. This is not as large as would be the case near a deep ocean if the continental lithosphere would in total be highly-resistive (i.e., resistivity in the order of 1000 Ωm or more). Thus the continent must generally be less resistive (a few hundred Ωm maximum) or must at least contain anomalous high-conductivity zones.

Given the average N10°E trend of the trench and the similar overall course of the volcanic chain, it was expected that real parts of induction vectors would show a general W-E tendency. This is, however, not the case. Instead, at long periods, all real induction vectors point systematically NE for all sites in the measuring area, regardless on which geological unit data were collected (Fig. 4.15). Note that there is not a single site in the study area where this observation is opposed. Thus flow of anomalous current in the continent – itself caused by current concentration in the ocean parallel to the coast – is not NS as would be the case for a simple 2-D distribution of conductivity, but obliquely deflected on a large lateral scale.

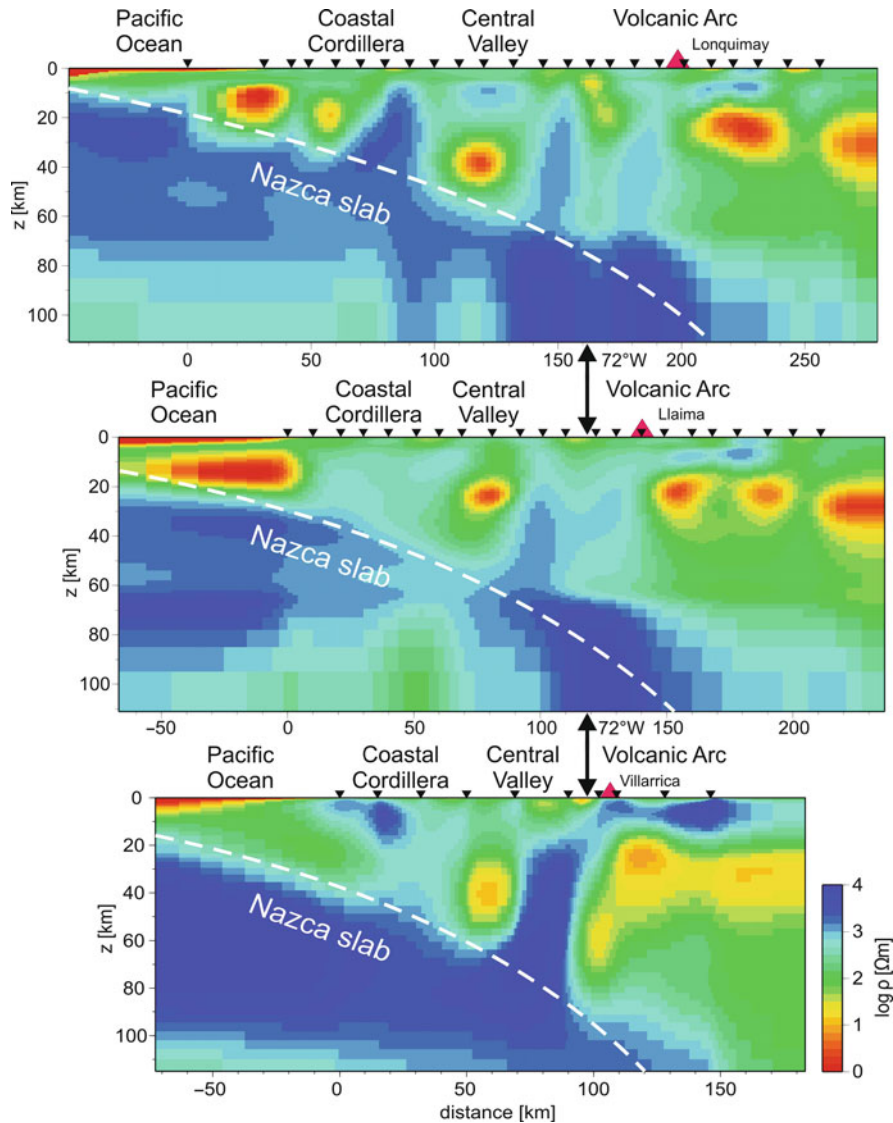


Fig. 4.14 Results of isotropic 2-D inversion of the northern, central and southern profiles in Southern Chile (Brasse et al. 2009, Montahei 2011, Kapinos 2011)

On the other hand, this effect is not observed at shorter periods: The coast effect is “normal” and vectors in the Coastal Cordillera point roughly perpendicularly away from the shoreline (not necessarily perpendicular to the trench, since local bathymetry is dominating at short periods). This also rules out an instrumental effect as we initially suspected (and which gave rise to a later extensive test program of stations near Niemegk geomagnetic observatory close to Berlin). Source effects should not play a significant role, too, because the study area is located in

mid-latitudes and far from both polar and equatorial electrojets.

An interesting effect is visible around highly active volcanoes Villarrica (altitude 2847 m) and Llama (3125 m, latest eruption in 2008), where a small network of sites was established: While induction vectors at 100–200 s point away from Villarrica at the closest sites, this is not seen at Llama. Although all volcanic edifices lead to a topographic effect at their slopes, this cannot be the reason for the direction and magnitude of vectors at Villarrica. Since the slope of this mountain is

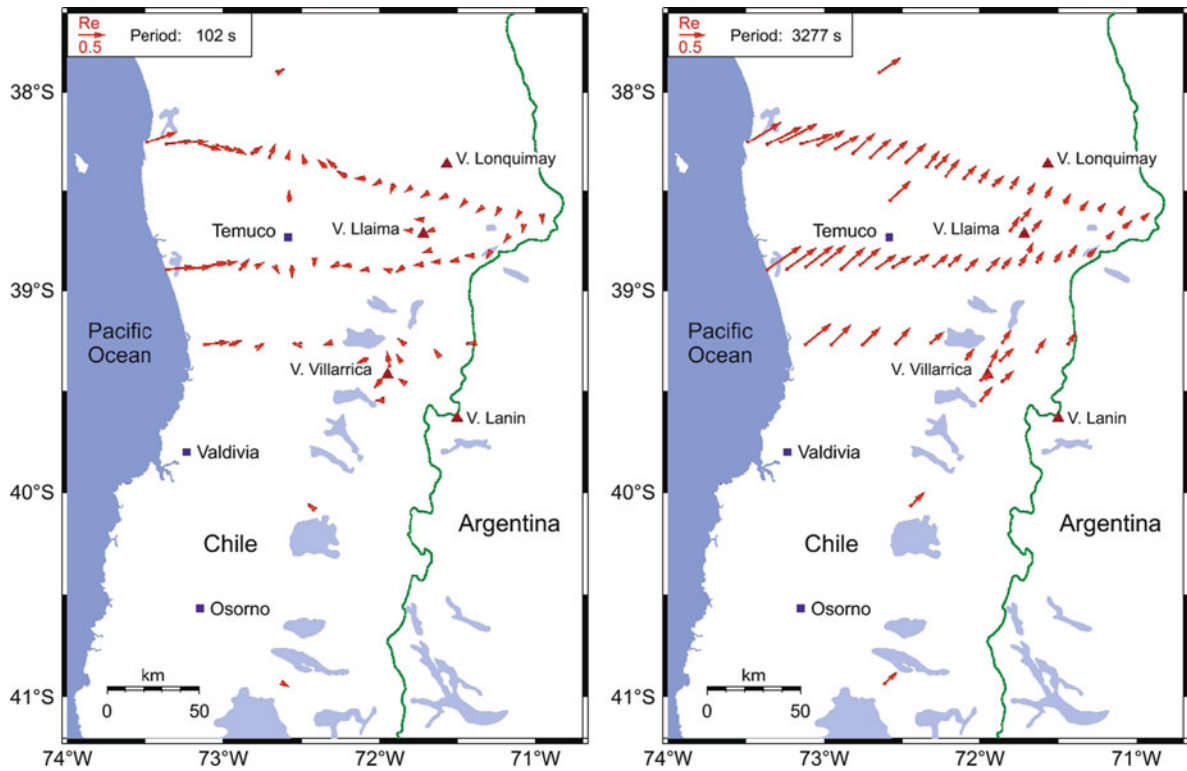


Fig. 4.15 Induction vectors in S. Chile at $T = 102$ s (left) and 3277 s (right)

only in the order of $25\text{--}30^\circ$, topography signals in MT transfer functions are restricted to short periods (<10 s) and only a static shift-like effect remains in apparent resistivities as was shown by 2-D and 3-D modeling of topographic effects in the central Andes (Bydam 2008, Brasse and Bydam 2008). We may thus assume that deeper in the crust beneath Villarrica a large-scale magma deposit might exist – note that the crater at the top of Villarrica is filled with a lava lake (Calder et al. 2004). A more detailed statement about conductivity distribution at depth below the volcano is not possible for the time being, since detailed 3-D modeling has not been carried out yet. Note that these long-period data only permit statements about the deeper crust; to assess a possible magma deposit just beneath the volcanic edifices would require measurements at shorter periods (AMT range) on a denser network.

4.3.2.3 3-D Modeling Attempts to Explain Induction Vectors

It is obvious that the anomalous deflection of induction vectors cannot be explained by pure 2-D models. We therefore tested several simple 3-D approaches to

account for the deflection over a large area, in particular the N-S extent of at least 350 km (it is not known if transfer functions continue to be this anomalous to the north and south of the measuring area, but this may quite safely be assumed at least for some distance). Such models must incorporate the Pacific Ocean with an average depth of ~ 4.5 km and an almost N-S running coastline, and some other structure of large, regional extent which accounts for the deflection. For the computations the algorithm of Mackie et al. (1994) was applied; seawater resistivity was fixed at $\rho = 0.3 \Omega\text{m}$.

Test 1: It may be possible that a layer with increasing conductance (conductivity-thickness product) from north to south exists at some depth in the crust or even in the upper mantle. This may indeed explain the induction vectors but leads to inherently large conductances in the northern part (and unrealistic conductivities if layer thickness is not changed accordingly). Furthermore there exists no geological evidence whatsoever for such a layer and the idea is thus abandoned here.

Test 2: South of the southernmost site begins archipelagic Chile, i.e., the Central Depression is submerged and the Coastal Cordillera becomes a chain of islands, with Isla de Chiloé being the largest (not shown in Fig. 4.12). The distribution of seawater masses causes therefore a deflection of induction vectors near latitude 41°S , but according to our model results this effect does not reach far enough to the north, taking the known water depths into account.

Test 3: At $45\text{--}46^\circ\text{S}$, i.e., 450–550 km south of the study area the Chile Rise is subducted beneath the continent; this is the triple junction between Antarctic, Nazca and South American plates. It may be speculated that the location of the triple junction is associated with a deep seated plume structure of enhanced conductivity. Such a hypothetical good conductor (resistivity $1\ \Omega\text{m}$) was incorporated into the 3-D model (which also takes the irregular coastline into account); the response is shown in Fig. 4.16. Again, the model response is only compatible with the data at the southernmost sites of the measuring area; in the north vectors point strictly W-E.

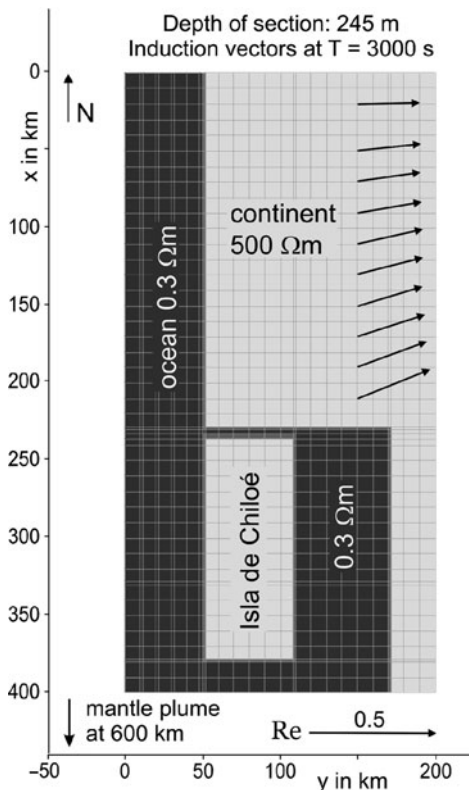


Fig. 4.16 One of the 3-D models calculated to explain deflection of induction vectors

Summarizing, simple and (geologically) realistic 3-D models explaining the observed induction vectors could not be found (which does of course not exclude more detailed classes of models, see later). We therefore tested another approach, the simulation of a deeply fractured crust with anisotropic 2-D models.

4.3.2.4 2-D Models with Anisotropy: Some Principal Considerations

Under anisotropy we may either understand micro-anisotropy as an inherent rock property or structural (pseudo- or macro-) anisotropy; in both cases the inductive scale length (“wave length”) of fields in the earth is larger than the width of individual structural units which are thus not resolvable separately. We may assign either one or two directions to high conductivity: The first case may be interpreted as simulating a system of line currents while the second may be regarded as an image of a sequence of fault planes. A ratio of $\gg 100$ between directions of low and high conductivity seems reasonable if we assign the resistive part to the host rock and the conductive one to possible fault planes, assumed to be fluid-rich in the damage zone of the fault core.

Full anisotropy has to account for 6 variables, the 3 principal resistivities, strike, dip and slant (Pek and Verner 1997). Due to the resulting complexity we varied only the first 4 parameters leaving dip and slant constant at 90° and 0° , respectively. Dip and slant (if not too large) have a much smaller influence on transfer functions than the other parameters. Since ρ_z has only minor influence on induction vectors at least distant from the coast, this quantity was set equal to ρ_x for most model experiments.

If an anisotropic layer – extending to infinity in horizontal directions – is present in an otherwise isotropic and homogeneous or layered half space, a split of impedance phases and apparent resistivities is observed while the vertical magnetic field is zero; the vertical components of the secondary field from the parallel current lines – or planes – superpose destructively. A vertical field only arises if the anisotropic layer is bounded or if some other lateral inhomogeneity is present, in our case mainly from the coast effect at the Chilean margin. Under 2-D isotropic conditions only the W_y component of the tipper would exist due to the basically N-S trending coastline and trench. Here, however, W_x is of similar magnitude at long periods.

First we evaluate the responses of several principal models for periods of $T = 102.4$ and 3277 s, respectively, corresponding to period bands at which transfer functions are estimated by the time series analysis scheme. We thus analyze responses at periods corresponding to relatively short and large penetration depths. Calculations were carried out employing the algorithms of Pek and Verner (1997) and Li (2002); both yield comparable results.

(1) An anisotropic layer between $z = 5$ and 20 km, bounded at $y = 20$ km and $y = 200$ km is embedded in a homogeneous half space of resistivity $300 \Omega\text{m}$. Resistivities of the layer are set to $\rho_x = \rho_z = 1 \Omega\text{m}$ and $\rho_y = 300 \Omega\text{m}$, anisotropy strike to $\alpha = 45^\circ$. The conductive axis thus strikes SW-NE. We neglect any non-zero dip or slant and simply assume vertical conductive planes. Vertical resistivity has only minor influence on the vertical magnetic field at the surface (in contrast to impedance, which we don't further investigate here) and only near the layer boundaries. At both margins of the anisotropic block significant induction vectors are observed, pointing NW in the west and SE in the east (i.e., both perpendicular to strike); above the center of the block the combined effect of both margins results in a vanishing vertical field. According to depth of penetration vectors are largest for shorter periods – for longer periods penetration depth increases and the layer is too shallow to have a major effect.

(2) Since the observed induction vectors display a significant W_x component from the coast until the Argentinian border, the anisotropy has to persist eastward beyond the station network. This is taken into account by removing the layer bound in the east. Because no data exist in Argentina at this latitude, we have no information on the eastern margin of the layer and simply set it to infinity. Furthermore, a large W_x component is present also at coastal site PUR and even at sea-bottom site OB7 20 km offshore on the northern profile (Kapinos 2011) as well as on Isla Mocha (O. Ritter, pers. comm.). Therefore the western margin has to be extended below the ocean; here it is arbitrarily set to $y = -20$ km. As expected, oblique induction vectors are only observed at the western margin, but now the effect is largest for long periods due to the infinite extent towards east.

(3) The Pacific Ocean is simulated by a conductive half layer with a thickness of 5 km. For the time being we neglect the actual bathymetry and place the block

at $y = -80$ km from the coast, i.e., 60 km away from the anisotropic layer. We also neglect dependence of seawater conductivity on salinity and temperature (i.e., water depth) and set it to an average value of $\sigma = 3.3 \text{ S/m}$ ($\rho = 0.3 \Omega\text{m}$).

The third model already grossly explains the observed induction vectors at long periods: They point NE over the whole profile, slowly decreasing in length with distance from the ocean. This behavior is not difficult to understand: If ocean and anisotropic layer are separated far enough from each other and thus not coupled, we may simply carry out a vector addition of contributions originating from the ocean and the layer, respectively. Accordingly the E-pointing “ocean vector” and the NW-directed “anisotropy vector” yield a combined vector pointing towards NE. Both real parts of W_x and W_y are positive in this case. At short periods the ocean effect is smaller due to the distance from the ocean with its crude geometry adopted here (note that this characteristic does not conform with observation and a more realistic bathymetry has to be incorporated; see below). Imaginary parts remain small in all cases, they are discussed later.

If, however, the anisotropic layer extends below the ocean, the anomalous fields of both structures will be coupled. Then a simple vector addition does not suffice; e.g., the secondary field of the anisotropic layer induces a “secondary secondary” field in the ocean which is no longer N-S but rather obliquely oriented with respect to the coast. This is taken into account by the modeling algorithm. For further discussion on coupled anomalies in the anisotropic case see, e.g., (Weidelt 1999) and (Soyer 2002).

From these fundamental considerations it is immediately evident, that the anisotropy strike does *not* reflect the NW-SE oriented fault pattern as displayed in Fig. 4.12. Highly conductive planes in that direction would produce SE-oriented induction vectors; thus information from tippers reveals other, less obvious structures (see discussion below).

(4) As already mentioned above, the uniform pattern of induction vector deflection is only observed at periods >1000 s, while at shorter periods local effects come into play. In a 4th test we thus shifted the anisotropic layer into the lower crust, i.e., it is located now between 20 and 38 km. This approach also reproduces the oblique vectors and differences to the responses of model (3) are only minor. It is thus difficult to discriminate between upper and lower crustal

anisotropy from one period alone, and the full period range has to be taken into account.

4.3.2.5 Anisotropic Models for the Chilean Margin

Due to the large number of parameters involved when carrying out 2-D anisotropic modeling, the search for a model that fits real and imaginary tippers at all sites for all frequencies, and that is preferably somehow geologically realistic is a time-consuming issue. Like in the preceding section we set slant, dip to constant values and varied only ρ_x , ρ_y (with $\rho_z = \rho_x$) and anisotropy strike α plus the isotropic background resistivities. Some of the features of the isotropic 2-D inversion results (see Fig. 4.14) were incorporated and adjusted where necessary.

The resulting model is displayed in Fig. 4.17 – calculated for the central profile of Fig. 4.12. It incorporates a homogeneous background with a resistivity of 200 Ωm , an anisotropic layer in the lower crust and the Pacific Ocean with detailed bathymetry, taken from ETOPO1 data and swath bathymetry obtained during several cruises of RV Sonne (Scherwath et al. 2006). The subducting oceanic Nazca slab is modeled as a poor conductor with a vertical extent of 150 km (lower limit not shown in Fig. 4.9). The dip angle of the slab is provided by seismological studies (Bohm et al. 2002, Yuan et al. 2006) and the TIPTEQ seismic transect along the northern MT profile (Groß et al. 2007).

The trench contains a sediment filling with a thickness of about 2 km (Völker et al. 2006) and with presumably low (but unknown) resistivity. The filling and its geometry – known from offshore reflection seismology, e.g., Sick et al. (2006) – is roughly taken into account by assigning an arbitrary low resistivity (5 Ωm), which suffices if only onshore (i.e., far away) stations are investigated. The same resistivity is set for the uppermost oceanic crust. We used also information from the isotropic inversion; particularly the near surface structures are motivated by isotropic models and allowed to fit at least in a crude manner the short-period induction vectors. On the other hand the compatibility between the isotropic and anisotropic models shows that they complement rather than oppose each other.

We carried out numerous tests to constrain upper and lower boundaries of the anomalous, anisotropic layer. Without going into further detail here it may be concluded that one cannot resolve (as might be expected) the thickness of the anisotropic layer; in our model it reaches until Moho depths. The crust-mantle boundary lies at 35–45 km depth in South Chile as inferred from seismological studies, e.g., Krawczyk et al. (2006) and Asch et al. (2006). Since the deflection of induction vectors persists for offshore stations until the trench (Kapinos 2011), the anisotropic layer may not be located at mantle depths, because the downgoing slab would cut this layer apart. It is additionally not easy to constrain the upper limit of the

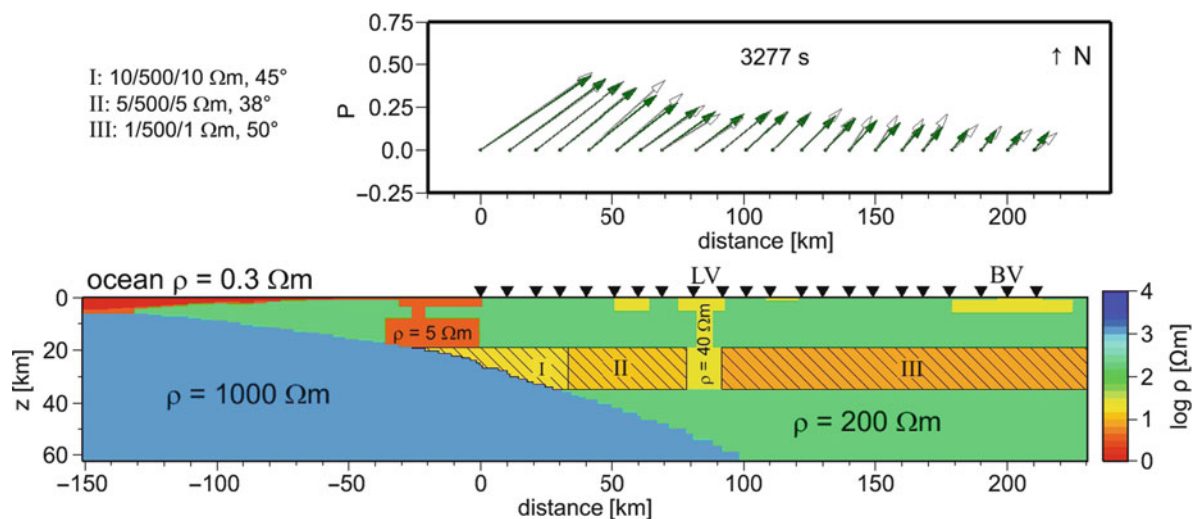


Fig. 4.17 Bottom: Anisotropic 2-D model for Southern Chile. Top: Measured (open arrows) induction vectors and model response (filled arrows)

layer since, at short periods, induction vectors show more local (also 3-D) features which are difficult to implement.

It would be unrealistic to assume that in a subduction zone setting (considering the movement of plates, resulting stress field and the oblique faults traversing the study area) the anisotropic layer will stay intact (unharmed) at the regional scale. It is rather to expect that features like resistivity or strike direction will change along the profile and which will also be reflected in the induction vectors. Indeed, the best fitting is obtained by dividing the anomalous layers in sections with minor variations in the anisotropic parameters. The values of resistivities in x-, y- and z-directions and the strikes are shown in Fig. 4.17. The ocean primarily accounts for the length of induction vectors near the coast while the strike of anisotropy is responsible for the deflection from W-E. The minimum of vector lengths at ~ 75 km may be accounted for by introducing a homogeneous and isotropic block at the location where the profile crosses the Lanalhue Fault, in accordance with the isotropic inversion results.

In the model of Fig. 4.17 this anisotropy strike – i.e., the conductive axis – is basically running NE-SW. This strike direction is also motivated by the horizontal stress field and lineaments of minor eruptive centers along the Liquiñe-Ofqui lineament (López-Escobar et al. 1995), which is discussed later.

Note that MT and GDS data are usually measured in geomagnetic coordinates and the coordinate system used here is set accordingly. Since the declination of the main geomagnetic field is in the order of $N10^\circ E$ (incidentally similar to the direction of the trench and the volcanic chain), it has to be taken into account when comparing geomagnetic results with geographic directions. A geomagnetic strike direction of 50° thus corresponds to geographic $N60^\circ E$.

Also note that anisotropy persists along the whole profile and extends below the volcanic arc (where induction vectors are small but still deflected) and even into Argentina, east of the easternmost site location. Introducing an isotropic good conductor below or to the east of the profile levels the amount of induction vectors and debases the fitting considerably. The model in Fig. 4.17 also includes near-surface, well-conducting sediments ($\rho = 40 \Omega m$ with a very thin layer of resistivities of $10 \Omega m$ on top, which is not visible in the plot) in the Central Depression and the Bío-Bío valley. The thickness of these sediments is not

known and was arbitrarily set to 2 km. Finally, apart from responses at short periods (and at long periods for the imaginary part) the data fit is reasonable (Brasse et al. 2009).

We can of course not rule out that a certain degree of anisotropy exists in the uppermost continental mantle or in parts of the upper crust. In the 1st case this is not resolvable, in the 2nd case a possible difference between ρ_x and ρ_y could be so small that it has only negligible influence. We may also discard a possible anisotropy of the oceanic crust (which might intuitively be the case due to the numerous fracture zones entering the subduction system) as the cause for induction vector deflection – model studies showed that its influence would not reach far enough along the profile on the continent.

4.3.2.6 Discussion of Models in South Chile

The deduced overall preference direction of electrical conductivity (NE-SW) does not agree with the image of faults in the South-Central Andes, striking obliquely (NW-SE) to the continental margin as shown in Fig. 4.12 (Melnick et al. 2006), as could originally be suspected. Apart from the Lanalhue Fault – consistently modeled as a good conductor in both isotropic and anisotropic approaches – the strike direction in the lower crust is rather perpendicular to the overall forearc fault pattern. The (structural) deep-crustal anisotropy also crosses the most prominent mega shear zone in Chilean Northern Patagonia, the $\sim N10^\circ E$ striking Liquiñe-Ofqui Fault Zone (LOF) which extends from the triple junction area at $\sim 46^\circ S$ until $38^\circ S$, where it terminates at the Bío-Bío-Aluminé Fault (BBAF). The LOF is assumed to largely control volcanism in S. Chile (e.g., Cembrano et al. 1996) because many of the Quaternary and active volcanoes are aligned along this lineament.

The structural anisotropy has to continue eastwards across the border into Argentina for at least several tens of kilometers, perhaps until the backarc volcanic centers of the Loncopué trough. The lateral extent to the east cannot be constrained, as there are no stations at this latitude in Argentina (the closest stations from the University of Washington and INGEIS Buenos Aires are still several hundred km to the north; J.R. Booker and C. Pomposiello, pers. comm.). On the other side of the Andean range, the anisotropy reaches most likely until the plate interface, at least significantly beneath the Pacific Ocean. The N-S extension of the anomalous

zone is again not known due to missing data N of 38°S and S of 41°S.

A hint at the cause of the structural anisotropy comes from an early observation by (Nakamura 1977): Different from the ~N10°E alignment of the large stratovolcanoes along the LOF, minor eruptive centers, parasitic vents and flank craters in the Central Southern Volcanic Zone are predominantly aligned in a NE-SW direction. Nakamura (1977) related this preference direction to the maximum horizontal stress S_H in the arc region and assumed a system of dikes enabling the rise of molten or partially molten material to the surface. López-Escobar et al. (1995) and Muñoz et al. (2000) refined this study by analyzing the geochemistry of rocks and their source region. Indeed, most of the samples they analyzed are of mainly basaltic composition (in contrast to the more andesitic-basaltic composition of the large stratovolcanoes), indicating a short residence time of magmas in the crust. The generally NE-SW oriented stress in this part of the Chilean margin (Assumpção 1992) was recently confirmed by Reuther and Moser (2007) for the uppermost crust until depth of ~500 m. The analysis of 2nd order structures (lineaments, dikes, drainage anomalies) by Rosenau et al. (2006) gives further evidence of the importance of the NE-SW direction.

According to Shaw (1980) dikes in the crust develop perpendicular to the direction of minimal effective stress (S_3). The maximum horizontal stress may then either be S_1 or S_2 . In a strike-slip environment (like the Southern Volcanic Zone) S_1 and S_3 are horizontal while S_2 is vertical, thus allowing partial melts and fluids to rise in vertical dikes, parallel to S_H . Local features (e.g., gravitational load from the stratovolcanoes and the mountain range as such) may modify the overall stress pattern – this may in turn lead to local deviations of induction vector directions and to slightly different conclusions on anisotropy directions along the 3 profiles in the study area.

Our findings concerning structural anisotropy (if we regard it as a measure of a deeply fractured crust, but being unable to resolve individual dikes/faults due to wavelength considerations) strongly support the assumption of Nakamura (1977) and López-Escobar et al. (1995). The surprising result is, however, that the crust has to be deeply fractured in the forearc as well. Due to low temperatures in the forearc crust the conductive phase cannot be any partial melt here – instead we have to assume a relatively cold, but

fluid-rich crust or even, at least partly, an occurrence of metallic phases. The extension of anisotropy beneath the Coastal Cordillera would be in accordance with the broadening of the mid-Tertiary volcanic arc until the Pacific coast, where volcanic outcrops occur south of our actual study area at 41°S (Muñoz et al. 2000). Our results suggest that this magmatic event may have reached even further to the west, beyond the coastline and perhaps until the continental slope.

Unfortunately the model in Fig. 4.17 explains the impedances only in a crude manner. For the time being we have been unable to construct a model which satisfactorily fits both magnetotelluric and vertical magnetic field observations; this constitutes the next task for the evaluation of the data set. However, several features of the model presented here correspond to the isotropic impedance model (Brasse and Soyer 2001), in particular the enhanced conductivity below the Central Depression and the generally higher conductivities beneath the volcanic arc. The characteristics of induction vectors outside the area depicted in Fig. 4.12 are not known and it would thus be a rewarding effort to establish further sites to the north of the Bío-Bío Fault and to the south in archipelagic Chile.

4.4 Magnetotelluric Studies in Central America

In the Central American subduction zone, the Cocos Plate subducts slightly obliquely in a northeastern direction beneath the Caribbean Plate with a convergence rate of ~8.5 cm/a (DeMets 2001). Depth of the Middle America Trench (MAT) gradually decreases from offshore Nicaragua ($z > 5000$ m) to less than 2000 m in southern Costa Rica, where the Cocos Ridge is subducted. Similarly, the subduction angle decreases from near vertical beneath Nicaragua to sub-horizontal beneath S Costa Rica (Protti et al. 1995, Husen et al. 2005), implying a significant diversity in the geothermal regime (Peacock et al. 2005). The varying slab dip is seen as a result of differences in the strength of the mantle wedge beneath Nicaragua and Costa Rica (Rychert et al. 2008). The position of active arc volcanoes above the downgoing slab changes abruptly near the border between the two countries: While volcanoes in the Cordillera de Guanacaste of NW Costa Rica are located roughly above the 100 km depth contour line, Nicaraguan volcanoes sit above a

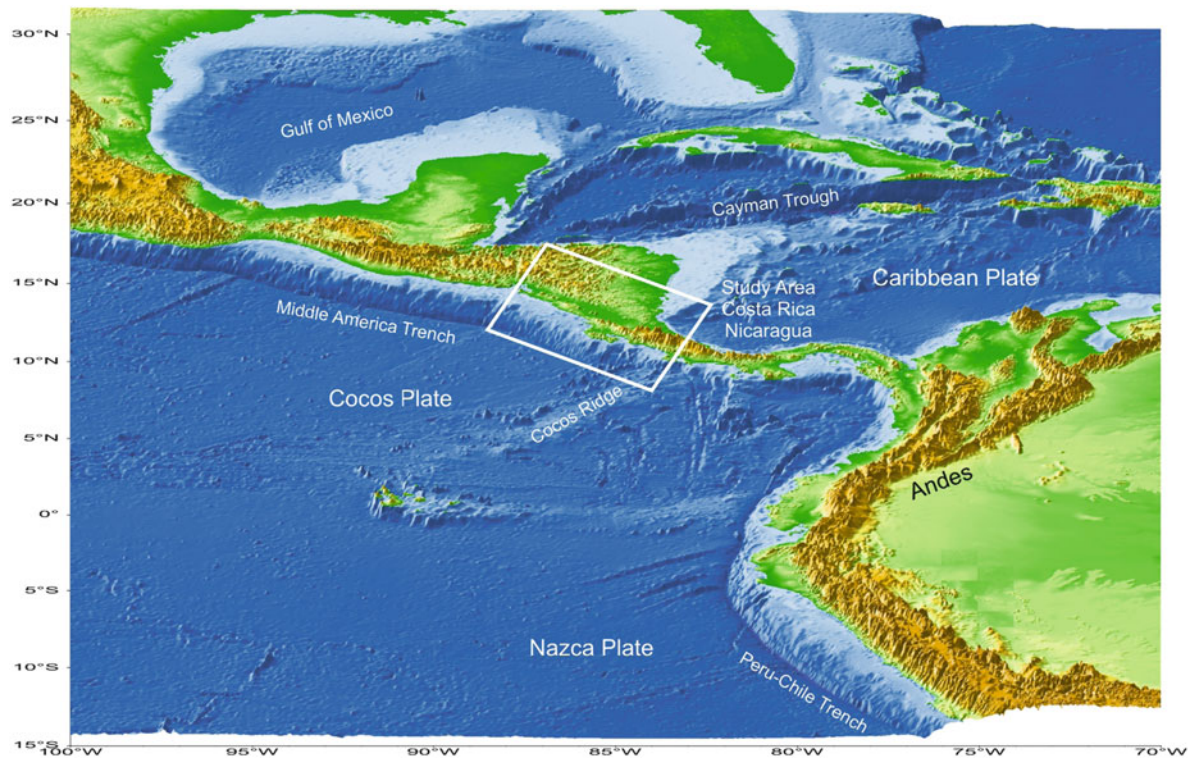


Fig. 4.18 Setting of Central America. Topography and bathymetry are plotted from ETOPO1 data

much deeper segment (>150 km) of the Cocos plate (Syracuse et al. 2008). A significant variation of lava chemistry is observed, with larger fluid and sediment signature beneath Nicaragua than beneath Costa Rica (Carr et al. 2003, Rüpke et al. 2002). Additionally, crustal thickness beneath the Costa Rican arc is significantly larger (~ 38 km) than beneath the Nicaraguan depression (~ 25 km) [79].

The Pacific margin of Central America has in the recent past been studied intensively, particularly with seismological (on- and offshore) and geochemical methods; it is a key location of the NSF Margins Program and also addressed by a number of projects funded by the German Science Foundation. We present here the first results of a complimentary project which aims to investigate the electrical resistivity distribution at the margin by employing long-period ($T = 10 - 10^4$ s) magnetotelluric and geomagnetic deep sounding (MTS and GDS). Data along a first profile comprising 18 sites with a spacing of ~ 10 km were collected in February/March 2008. It extends from the Pacific coast near Sámara, crosses the volcanic arc at Tenorio volcano and ends in the backarc near the Nicaraguan

border at Los Chiles (see Fig. 4.18), and coincides with the line of an active seismic experiment (e.g., (Sallarès et al. 2001)) and the TUCAN seismological study (e.g., Mackenzie et al. 2008).

Further relevant geological structures which are traversed by the MT line (and which are expected to have a response on the transfer functions) are the mafic and ultramafic rocks (ophiolites) of the Nicoya Peninsula (Hauff et al. 2000, Hoernle and Hauff 2000) and the sedimentary basins in the fore- and backarc, i.e., the Tempisque and San Carlos Basins. Here a few drillings – mainly carried out for hydrocarbon exploration – provide some constraints on the structure of these basins (Barboza et al. 1997, Pizarro 1993). In the backarc the profile crosses the so-called “Santa Elena suture”, extending from the peridotite outcrops of Santa Elena Peninsula in an easterly direction where it may connect with the Hess Escarpment as a major bathymetric step in the Caribbean plate and limit of the Caribbean Large Igneous Province. The Santa Elena suture is believed by some authors to mark the boundary between allochthonous Chortis and Chorotega blocks. Note, however, that this interpretation is



Fig. 4.19 MT sites in Central America (Costa Rica and Nicaragua)

contended (see discussion in Gazel et al. 2006, Mann et al. 2007). The Chortis block is apparently a continental fragment, while the Chorotega block is probably a continuation of the Caribbean LIP.

4.4.1 Data Characteristics

Data processing was carried out by employing the robust remote-reference scheme of Egbert (1997), which yielded mostly high-quality estimates of impedance and tipper in the period range $10\text{--}10^4$ s. A crucial step for further investigation is the check if the transfer functions reflect a two-dimensional (2-D) subsurface or if three-dimensional (3-D) structures are required by the data. As can be seen from Fig. 4.20

(top), the assumption of two-dimensionality is roughly but not completely fulfilled. Electrical strike directions – calculated from the impedances after Smith (1995) – for the entire profile are shown in Fig. 4.20 (note the 90° -ambiguity inherent to impedances; the decision for the true strike may be based on geology or tipper information). Data are split into three period bands (short, intermediate and long) and show basically similar characteristics: The strike is between $N45^\circ W$ and $N55^\circ W$ with a slightly larger scatter at short periods (10–100 s). This scatter is not surprising, as the influence of near-surface anomalies is larger for short periods. Additionally, for near-coastal sites, the bending of the coastline (which is not parallel to the trench) becomes relevant. Summarizing, the impedance data suggest that a 2-D approach is suitable

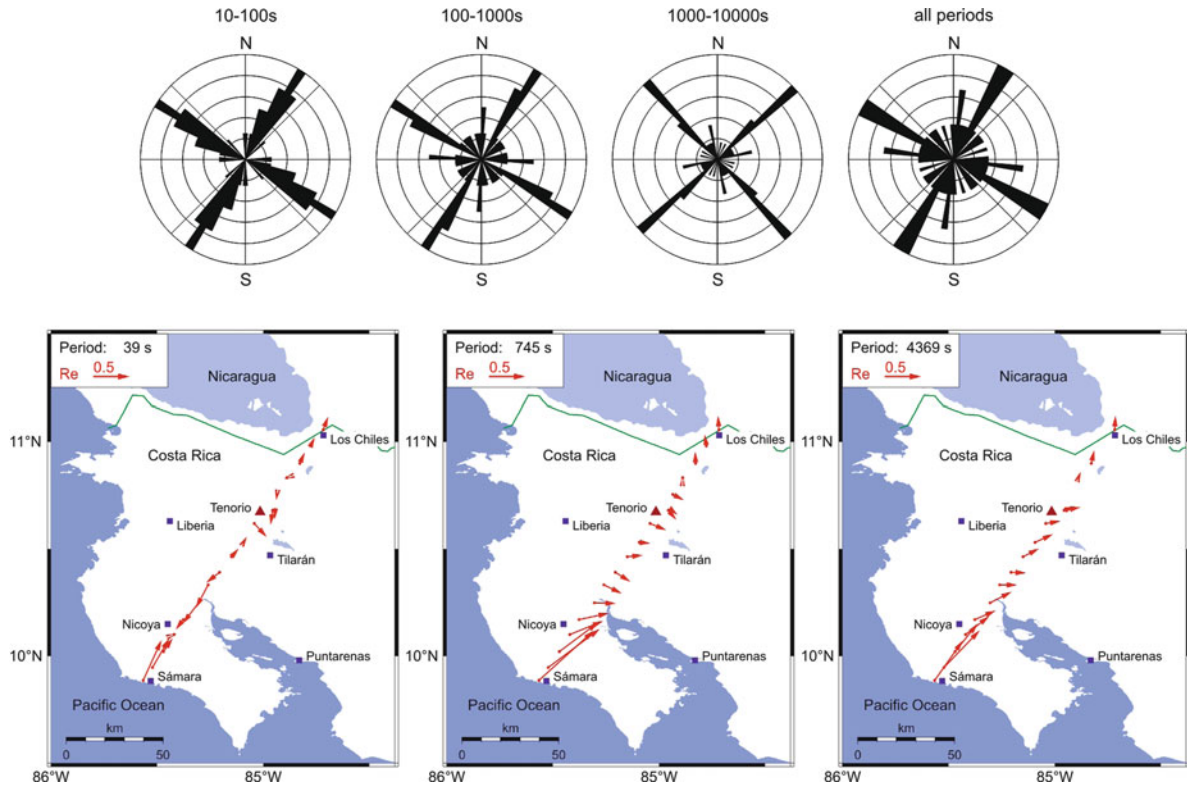


Fig. 4.20 Electrical strikes directions (*top*) and induction vectors (*bottom*) in Costa Rica

and the resulting strike is approximately perpendicular to the profile.

This clear statement is obscured somewhat by the induction arrows or vectors, as shown in Fig. 4.20 (bottom) for three periods. Induction arrows are calculated from the tipper; their real parts (\mathbf{P}) point towards or away from high conductivity zones (at least in simple environments), depending on convention. We use the latter here, and consequently at the coast arrows point away from the well-conducting ocean. This coast effect reaches a large magnitude of over 1.1 at site *sam* for periods between 1000 s and 2000 s, which is due to the proximity of the 4 km-deep trench off Nicoya, an effect which is enhanced by the relatively resistive ultramafic rocks of the peninsula. Interestingly the coast effect does not reach far inland; it is obviously compensated by the sediments of the Tempisque Basin and perhaps another, deeper anomaly. Near Tenorio volcano (site *par*) arrows do not point away from the edifice at short periods, but rather hint at a conductive zone farther to the west, i.e., Miravalles volcano (where a large geothermal reservoir is encountered). Even more evident is the deviation of arrows in the

Tempisque Basin itself at longer periods. This may either be caused by still deeper sediments in the NW or could even be attributed to the deepening of the trench near northernmost Costa Rica and off Nicaragua.

Thus induction vectors sense significant 3-D effects along the profile. One may argue that these arrows pointing perpendicularly to the profile in the center of the basin do not pose a problem for 2-D modeling; the projected arrows are almost zero and do not require a conductive structure directly beneath the line. Nevertheless, care must be taken when interpreting the following 2-D model.

4.4.2 Results of 2-D Modeling in NW Costa Rica

Taking the strike angle analysis and the direction of most induction arrows into account, we rotated all data by -53° , i.e., basically assuming a strike perpendicular to profile direction. As for the Andes data, the common non-linear conjugate gradient algorithm of Rodi and Mackie (2001) was used, which implements a

Tikhonov-type, regularized 2-D inversion scheme. The program allows for a multitude of settings with respect to regularization factor, weighting functions penalizing horizontal or vertical structure, and error floors, among others.

A number of tests were carried out to check dependence on starting models and inversion parameters. For the model shown in Fig. 4.21 crude bathymetry was included; seawater was given a fixed resistivity of $0.3 \Omega\text{m}$. Additionally, the oceanic lithosphere was set as a resistive feature with a resistivity of $1000 \Omega\text{m}$. The factor β was set to 1 (implying equal horizontal and vertical smoothing), and the regularization parameter was set to a value of 10 after a trade-off analysis between misfit and model roughness. To reduce the influence of static shift effects, error floors were set to higher values for apparent resistivities than for phases. All possible combinations of data sets were tested; the model of Fig. 4.21 was obtained by joint inversion of tipper, TE and TM mode data. The resulting model yields an rms of 2.09, while the inversion of individual modes shows smaller values (better fits) of around 1.3 to 1.5. This is to be expected and may be regarded as a sign for inherent three-dimensionality. However, the most relevant features of the model in Fig. 4.21 are recovered by all runs and a combination of TE, TM and tipper data. Data and model response are shown in the auxiliary material.

The crust beneath Nicoya Peninsula (structure A) is resistive (several hundred Ωm), but not as much as could be expected from its geological setting with predominantly mafic and ultramafic rocks, which should

display resistivities in the order of $1\,000 \Omega\text{m}$ and more. This may hint at a certain fluid input from the downgoing slab (see discussion later). The fore- and backarc basins (B_1 and B_2) are well resolved; thickness of conductive sediments corresponds to results of drillings in the vicinity of the MT line. In the Tonjibe borehole (San Carlos Basin) ultramafic rocks – similar to those outcropping in Santa Elena peninsula – constitute the basement at a depth of $\sim 2 \text{ km}$ (Pizarro 1993). In the Tempisque Basin well-conducting sediments seem to reach slightly larger depths, perhaps with a maximum off-profile to the NW, as indicated by induction arrows.

The northeastern part of the section shows a poor conductor which rather abruptly terminates in the region of Caño Negro (D). This location agrees well with the proposed trace of the Santa Elena suture (compare, e.g., (Saltarès et al. 2001)), and may be regarded as the southern terminus of the Chortis block. Note, however, that (Mackenzie et al. 2008) place this boundary slightly further to the north in Nicaragua. Interestingly the mid- and lower crust in northern Costa Rica is underlain by a good conductor (E). It may have a connection (conductive path) to the upper mantle, slightly NE of the volcanic chain and thus already in the backarc (E'). An upper crustal conductor is visible just NW of Tenorio volcano beneath sites *ten* and *maq* (C). This may indicate a shallow magma deposit, but the lack of sites at the volcano edifice (where topographic gradients and dense rain forest limit accessibility) does not permit a more definite statement. In contrast, no enhanced conductivity is modeled at lower

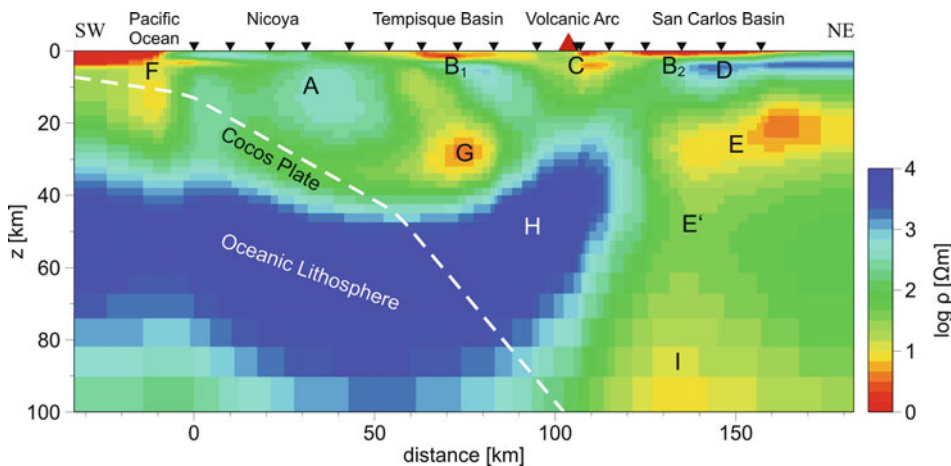


Fig. 4.21 2-D resistivity model for NW Costa Rica (Brasse et al. 2009)

crustal or upper mantle depth beneath the volcanic arc as was proposed by Elming and Rasmussen (1997) from the inversion of MT data in Nicaragua. Note, however, that Tenorio volcano is considered as dormant, unlike the highly active volcanoes in the Nicaraguan depression. This may be the consequence of the absence of a large magma deposit at depth.

Near-coastal conductive feature F in Fig. 4.21 poses a more severe problem for interpretation. It may be an inversion artifact (like the over-estimation of seafloor depth) as it is located seaward from and thus outside the profile (coastal site *sam* also has the worst fit, see electronic supplement). It may on the other hand signify a substantial fluid release from the slab and input into the crust, as was suggested for Central America from seismological observations due to bending-related faulting of the Cocos plate at the MAT (Ranero et al. 2003). Note that such a conductive feature seaward from the coastline appears in models of other subduction zones, too, for instance in South Chile (Brasse and Eydam 2008) and Cascadia (Soyer and Unsworth 2006). Without an offshore prolongation of the profile and ocean-bottom stations near the coast the resolution problems are difficult to overcome. Sea-bottom MT stations were deployed by IFM-Geomar (Kiel); these data are still under evaluation.

Note that the top of the slab (set resistive in the starting model) is changed to medium-resistive during the inversion process. The model in Fig. 4.20 is compatible with fluid release from the oceanic crust, serpentinization of the forearc mantle, and perhaps further dehydration further into the Caribbean plate (G). A serpentinized forearc mantle wedge beneath Nicoya has already been proposed by DeShon and Schwartz (2004) from seismological studies. Serpentine itself is probably only a moderate conductor (Bruhn et al. 2004). Thus structure G cannot be explained by serpentine alone; a free, interconnected fluid phase is necessary to explain the low resistivities in the order of 5–10 Ωm . This result concerning a fluid-rich forearc is in general agreement with seismological findings (Husen et al. 2003).

At depths between 40 and 90 km the plate interface and the Caribbean plate upper mantle have a similar high resistivity of several thousand Ωm (H in Fig. cr-model.jpg), comparable with the oceanic lithosphere and implying dry conditions throughout. Any occurrence of free fluids/melts is restricted to greater depth,

as can be deduced from the low resistivities in the asthenospheric wedge (I). Note that a postulated rise of fluids/melts from the asthenospheric wedge towards the volcanic arc (from I via E' to E and perhaps C) cannot be vertical or direct – H is a robust structure in the inversion process. It is generally compatible with a forearc mantle sliver found by Walther et al. (2000) further NW beneath Nicaragua and a zone of high velocities above the slab as inferred by Syracuse et al. (2008) from data of the recent TUCAN seismological experiment in Costa Rica and Nicaragua.

4.4.3 Results of Preliminary 2-D Modeling in Nicaragua

Investigation of the Nicaragua profile (B in Fig. 4.19) was conducted in early 2009. It extends from the coast of the Pacific Ocean, crosses the Nicaraguan Depression (where the narrow volcanic arc is located) and end in the Nicaraguan Highlands. Processing, strike and dimensionality analysis were performed in a similar manner as for the Costa Rica data and is not detailed here. The profile runs NW of an earlier study by Elming and Rasmussen (1997), who deduced a mid-crustal conductor beneath the Masaya volcanic complex south of Managua.

A preliminary 2-D model of the new profile is displayed in Fig. 4.22. As in Elming and Rasmussen (1997) a HCZ (anomaly B) is modeled beneath the volcanic arc (the profile passes between Momotombo and El Hoyo volcanoes), although slightly displaced to the NE. A connection (conductive path) to the upper mantle seems possible, indicating rise of fluids/melts; however, this structure is not very well resolved. The basin of the Nicaraguan Depression is a shallow conductive feature with a thickness of 2–3 km (A in Fig. 4.22). Again, the oceanic lithosphere is poorly conducting, this is also the case for the continental wedge beneath the coast (C).

A disturbing feature is the series of conductive “blobs” beneath the Nicaraguan Highland (question marks in Fig. 4.22). This was first believed to be a result of inadequate inversion parameter, but they also appear if the factor β in the inversion program (Rodi and Mackie 2001) which controls the balance of horizontal vs. vertical smoothing, is set to a higher value (e.g., 2 instead of 1 as was usually done). As in South Chile, this may hint at an anisotropic crust of the

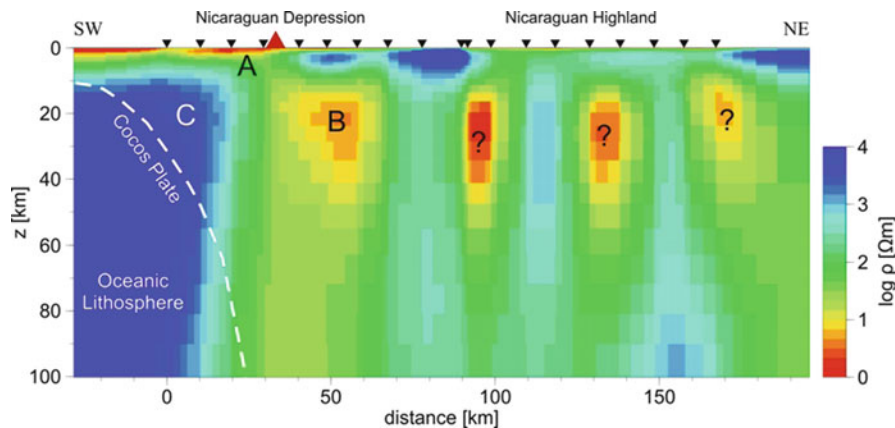


Fig. 4.22 Preliminary 2-D resistivity model for Nicaragua. Note the conductive “blobs”, marked with question marks: they appear even if strong horizontal smoothing is applied

Chortis block – these model experiments still have to be carried out.

4.4.4 Conclusion for Central America

Long-period magnetotelluric investigations resulted in the first deep resistivity image at the Costa Rica margin and an enhanced model in Nicaragua. Their principal features and implications are (a) the depth and low resistivity of the fore- and backarc basins, (b) the apparent termination of the Chortis block at the Santa Elena suture in northernmost Costa Rica, (c) a highly conductive backarc mid-crust and upper mantle, (d) the image of fluid release from the downgoing slab in the forearc, and (e) a very resistive forearc mantle adjacent to the subducted plate. These statements also hold for Nicaragua, where in addition a complicated (anisotropic) structure of the Chortis block is obvious. The resistivity image of fluid release from the downgoing slab is generally consistent with seismological observations. We assume hydrous fluids as a cause for the modeled resistivities in the forearc regions, as the temperature in the slab is probably too low to allow for partial melting. Partial melts may, however, occur in the asthenospheric wedge of the overriding plate and explain the high conductivities in the backarc.

The obtained resistivity cross-sections should be seen as a first order approximation. More field data are necessary to constrain 3-D effects – their collection and additional, comparative profiles in Nicaragua are planned in the near future. Incorporating the

sea-bottom MT data into the models will further contribute to the question of fluid content in the downgoing plate.

Acknowledgements The author wants to thank the partner institutions in Chile (Universidad Católica del Norte, Universidad de Concepción), Bolivia (Universidad Mayor de San Andrés), Argentina (Universidad Nacional de Salta, Universidad de Buenos Aires), Costa Rica (Instituto Costarricense de Electricidad) and Nicaragua (Instituto Nicaragüense de Estudios Territoriales); without their logistical support this work would not have been possible. The help of many members and students from these institutions and the Free University of Berlin is also gratefully acknowledged. Funding was provided by German Science Foundation (DFG) through numerous grants to the author.

References

- Aizawa K, Ogawa Y, Ishido T (2009) Groundwater flow and hydrothermal systems within volcanic edifices: delineation by electric self-potential and magnetotellurics. *J Geophys Res* 114:B01208. doi:10.1029/2008JB005910
- Allmendinger RW, Jordan TE, Kay SM, Isacks BL (1997) The evolution of the altiplano-puna plateau of the central andes. *Ann Rev Earth Planet Sci* 25:139–174
- ANCORP Working Group (2003) Seismic imaging of an active continental margin and plateau in the central Andes (Andean Continental Research Project 1996 (ANCORP '96)). *J Geophys Res* 108 doi:10.1029/2002JB001771
- Asch G, Schurr B, Bohm M, Yuan X, Haberland C, Heit B, Kind R, Woelbern I, Bataille K, Comte D, Pardo M, Viramonte J, Rietbrock A, Giese P (2006) Seismological studies of the central and southern andes. In: Oncken O et al. (eds) *The Andes: active subduction orogeny, frontiers in earth sciences*. Springer, Berlin, pp 443–458

- Assumpção M (1992) The regional intraplate stress field in South America. *J Geophys Res* 97:11889–11903
- Asters RC, Borchers B, Thurber CH (2005) Parameter estimation and inverse problems. *International Geophysics Series*, 90. Elsevier, Amsterdam
- Bahr K (1988) Interpretation of the magnetotelluric impedance tensor: regional induction and local telluric distortion. *J Geophys* 62:119–127
- Barboza G, Fernández JA, Barrientos J, Bottazzi G (1997) Costa Rica: petroleum geology of the Caribbean margin. *Lead Edge* 16:1787–1794
- Baumont D, Paul A, Beck S, Zandt G (1999) Strong crustal heterogeneity in the Bolivian Altiplano as suggested by attenuation of Lg waves. *J Geophys Res* 104:20287–20305
- Bohm M, Lüth S, Echtler H, Asch G, Bataille K, Bruhn C, Rietbrock A, and Wigger P (2002) The Southern Andes between 36° and 40°S latitude: seismicity and average seismic velocities. *Tectonophysics* 356:275–289
- Booker JR, Favetto A, Pomposiello MC (2004) Low electrical resistivity associated with plunging of the Nazca flat slab beneath Argentina. *Nature* 429:399–403
- Brasse H, Eydam D (2008) Electrical conductivity beneath the Bolivian Orocline and its relation to subduction processes at the South American continental margin. *J Geophys Res* 113:B07109. doi:10.1029/2007JB005142
- Brasse H, Kapinos G, Li Y, Mütschard L, Eydam D (2009) Structural electrical anisotropy in the crust at the South-Central Chilean continental margin as inferred from geomagnetic transfer functions. *Phys Earth Planet Inter.* doi:10.1016/j.pepi.2008.10.017
- Brasse H, Lezaeta P, Rath V, Schwalenberg K, Soyer W, Haak V (2002) The Bolivian Altiplano conductivity anomaly. *J Geophys Res* 107. doi:10.1029/2001JB000391
- Brasse H, Soyer W (2001) A magnetotelluric study in the Southern Chilean Andes. *Geophys Res Lett* 28:3757–3760
- Bruhn D, Siegfried R, Schilling F (2004) Electrical resistivity of dehydrating serpentinite. *Eos Trans AGU* 85(Fall Meet. Suppl):Abstract T41B-1176
- Cahill TA, Isacks BL (1992) Seismicity and the shape of the subducted Nazca Plate. *J Geophys Res* 97:17503–17529
- Calder ES, Harris AJL, Peña P, Pilger E, Flynn LP, Fuentealba G, Moreno H (2004) Combined thermal and seismic analysis of the Villarrica volcano lava lake, Chile. *Rev geol Chile* 31:259–272
- Caldwell TG, Bibby HM, Brown C (2004) The magnetotelluric phase tensor. *Geophys J Int* 158:457–469
- Carr MJ, Feigenson MD, Patino LC, Walker JA (2003) Volcanism and geochemistry in Central America: progress and problems. In: Eiler J (ed) *Inside the subduction factory*. *Geophysical Monograph Series*, vol 138. AGU, Washington, DC, pp 153–179
- Cembrano J, Hervé F, Lavenu A (1996) The Liquiñe Ofqui fault zone: a long-lived intra-arc fault system in southern Chile. *Tectonophysics* 259:55–66
- Cembrano J, Lavenu A, Yañez G, Riquelme R, García M, González G, Hérail G (2007) Neotectonics. In: Moreno T, Gibbons W (eds) *The geology of Chile*. Geological Society London, pp 231–261
- Chave AD, Constable SC, Edwards RN (1991) Electrical exploration methods for the seafloor. In: Nabighian MN (ed) *Electromagnetic methods in applied geophysics*, vol 2. Society of Exploration Geophysicists, Tulsa, pp 931–966
- Cifuentes I (1989) The 1960 Chilean earthquakes. *J Geophys Res* 94:665–680
- Comte D, Dorbath L, Pardo M, Monfret T, Haessler H, Rivera L, Frogneux M, Glass B, Meneses C (1999) A double-layered seismic zone in Arica, northern Chile. *Geophys Res Lett* 26. doi:10.1029/1999GL900447
- David C (2007) Comportamiento actual del ante-arco y del arco del codo de Arica en la orogénesis de los Andes centrales. PhD thesis, Universidad de Chile, Santiago
- Davies JH (1999) The role of hydraulic fractures and intermediate-depth earthquakes in generating subduction-zone magmatism. *Nature* 398:142–145
- DeMets C (2001) A new estimate for present-day Cocos-Caribbean plate motion: implications for slip along the central American Volcanic Arc. *Geophys Res Lett* 28:4043–4046
- DeShon HR, Schwartz SY (2004) Evidence for serpentinization of the forearc mantle wedge along the Nicoya Peninsula, Costa Rica. *Geophys Res Lett* 31. doi:10.1029/2004GL021179
- Diaz D (2010) Magnetotelluric investigation of the volcanic arc in the Central Andes with special emphasis on Lascar volcano. PhD thesis, Free University of Berlin
- Dorbath C, Granet M (1996) Local earthquake tomography of the Altiplano and the Eastern Cordillera of northern Bolivia. *Tectonophysics* 259:117–136
- Dorbath C, Masson F (2000) Composition of the crust and upper-mantle in the central Andes (19°30'S) inferred from P wave velocity and Poisson's ratio. *Tectonophysics* 327:213–223
- Egbert GD (1997) Robust multiple-station magnetotelluric data processing. *Geophys J Int* 130:475–496
- Elger K, Oncken O, Glodny J (2005) Plateau style accumulation of deformation: Southern Altiplano. *Tectonics* 24. doi:10.1029/2004TC001675
- Elming SA, Rasmussen T (1997) Results of magnetotelluric and gravimetric measurements in western Nicaragua, central America. *Geophys J Int* 128:647–658
- Engdahl ER, Villaseñor A (2002) Global seismicity: 1900–1999. In: Lee WHK, Kanamori H, Jennings PC, Kisslinger C (eds) *International handbook of earthquake and engineering seismology*, part A. Academic Press, Burlington, MA, pp 665–690
- Evans RL, Chave AD, Booker JR (2002) On the importance of offshore data for magnetotelluric studies of ocean-continent subduction systems. *Geophys Res Lett* 29. doi:10.1029/2001GL013960
- Eydam D (2008) Magnetotellurisches Abbild von Fluid- und Schmelzprozessen in Kruste und Mantel der zentralen Anden. Diploma thesis, Fachrichtung Geophysik, FU Berlin
- Folguera A, Zapata T, Ramos VA (2006) Late Cenozoic extension and the evolution of the Neuquén Andes. In: Kay SM, Ramos VA (eds) *Evolution of an Andean margin: a tectonic and magmatic view from the Andes to the Neuquén Basin (35°–39°S lat)*. *Geol Soc Am Spec Paper* 407. doi:10.1130/2006.2407(12)
- Friedel S (1997) Elektromagnetische Tiefensondierungen in Nordchile unter Berücksichtigung der Sq-Variationen und des EEJ. Diploma thesis, Fachrichtung Geophysik, FU Berlin

- Gaetani GA, Grove TL (2003) Experimental constraints on melt generation in the mantle wedge. In: Eiler J (ed) *Inside the subduction factory*. Geophysical Monograph vol 138. American Geophysical Union, Washington, DC pp 107–133
- Gaillard F (2004) Laboratory measurements of electrical conductivity of hydrous and dry silicic melts under pressure. *Earth Planet Sci Lett* 218:215–228
- Gaillard F, Malki M, Iacono-Marziano G, Pichavant M, Scaillet B (2008) Carbonatite melts and electrical conductivity in the asthenosphere. *Science* 322. doi:10.1126/science.1164446
- Gazel E, Denyer P, Baumgartner PO (2006) Magmatic and geotectonic significance of Santa Elena Peninsula, Costa Rica. *Geol Acta* 4:193–202
- Glodny J, Echtler H, Figueroa O, Franz G, Gräfe K, Kemnitz H, Kramer W, Krawczyk C, Lohrmann J, Lucassen F, Melnick D, Rosenau M, Seifert W (2006) Long-term geological evolution and mass-flow balance of the South-Central Andes. In: Oncken O et al. (eds) *The Andes: active subduction orogeny, frontiers in earth sciences*. Springer, Berlin, pp 401–428
- González-Ferrán O (1994) *Volcanes de Chile*. Instituto Geográfico Militar, Santiago de Chile, 640pp
- Groß K, Micksch U, TIPTEQ Research Group, Seismics Team (2007) The reflection seismic survey of project TIPTEQ – the inventory of the Chilean subduction zone at 38.2°S. *Geophys J Int*. doi:10.1111/j.1365-246X.2007.03680.x
- Grove TL, Chatterjee N, Parman SW, Médard E (2006) The influence of H₂O on mantle wedge melting. *Earth Planet Sci Lett* 249:74–89
- Haberland C, Rietbrock A, Lange D, Bataille K, Hofmann S (2006) Interaction between forearc and oceanic plate at the south-central Chilean margin as seen in local seismic data. *Geophys Res Lett* 33. doi:10.1029/2006GL028189
- Haberland C, Rietbrock A, Schurr B, Brasse H (2003) Coincident anomalies of seismic attenuation and electrical resistivity beneath the southern Bolivian Altiplano plateau. *Geophys Res Lett* 30. doi:10.1029/2003GL017492
- Hacker BR, Peacock SM, Abers GA, Holloway SD (2003) Subduction factory, 2. Are intermediate-depth earthquakes in subducting slabs linked to metamorphic dehydration reactions? *J Geophys Res* 108. 10.1029/2001JB001129
- Hamza VM, Muñoz M (1996) Heat flow map of South America. *Geothermics* 25:599–646
- Hauff F, Hoernle K, van den Bogaard P, Alvarado G, Garbe-Schönberg D (2000) Age and geochemistry of basaltic complexes in western Costa Rica: contributions to the geotectonic evolution of Central America. *Geochem Geophys Geosyst* 1. doi:10.1029/1999GC000020
- Heise W, Caldwell TG, Bibby HM, Bennie SL (2010) Three-dimensional electrical resistivity image of magma beneath an active continental rift, Taupo Volcanic Zone, New Zealand. *Geophys Res Lett* 37:L10301. doi:10.1029/2010GL043110
- Heise W, Pous J (2001) Effects of anisotropy on the two-dimensional inversion procedure. *Geophys J Int* 147: 610–621
- Heit BS (2005) *Teleseismic tomographic images of the Central Andes at 21°S and 25.5°S: an inside look at the Altiplano and Puna plateaus*. PhD thesis, FU Berlin
- Hérail G, Rochat P, Baby P, Aranibar O, Lavenue A, Masclez G (1997) El Altiplano Norte de Bolivia, evolución geológica terciaria, El Altiplano: ciencia y conciencia en los Andes, Actas 2. In: Charrier R et al. (eds) *Simposio Internacional Estudios Altiplánicos*, Arica 1993. Universidad de Chile, Santiago, pp 33–44
- Hildreth W, Moorbath S (1988) Crustal contributions to arc magmatism in the Andes of central Chile. *Contrib Mineral Petrol* 98:455–489
- Hill GJ, Caldwell TG, Heise W, Chertkoff DG, Bibby HM, Burgess MK, Cull JP, Cas RAF (2009) Distribution of melt beneath Mount St Helens and Mount Adams inferred from magnetotelluric data. *Nat. Geosci.* doi:10.1038/NNGEO661
- Hoernle K, Hauff F (2000) Oceanic igneous provinces. In: Burschuh J, Alvarado GE (eds) *Central America: geology, resources, hazards*, vol 1. Taylor & Francis, London, pp 523–548
- Husen S, Quintero R, Kissling E, Hacker BR (2003) Subduction zone structure and magmatic processes beneath Costa Rica as constrained by local earthquake tomography and petrologic modeling. *Geophys J Int* 155:11–32
- James DE (1971) Andean crustal and upper mantle structure. *J Geophys Res* 76:3246–3271
- James DE, Sacks JW (1999) Cenozoic formation of the central Andes: a geophysical perspective. In: Skinner B (ed) *Geology and ore deposits of the central Andes*. Society of Economic Geologists Special Publication 7, Littleton, CO, pp 1–25
- Jiracek G, Curtis J, Ramirez J, Martinez M, Romo J (1989) Two-dimensional magnetotelluric inversion of the EMSLAB lincoln line. *J Geophys Res* 94:14145–14151
- Jödicke H, Jording A, Ferrari L, Arzate J, Mezger K, Rüpke L (2006) Fluid release from the subducted Cocos plate and partial melting of the crust deduced from magnetotelluric studies in southern Mexico: implications for the generation of volcanism and subduction dynamics. *J Geophys Res* 111. doi:10.1029/2005JB003739
- Kapinos G (2011) *Amphibious magnetotellurics at the South-Central Chilean continental margin*. PhD thesis, Free University of Berlin
- Kay SM, Mpodozis C (2001) Central Andean Ore deposits linked to evolving shallow subduction systems and thickening crust. *GSA Today* 11:4–9
- Kirby SH, Engdahl ER, Denlinger R (1996) Intermediate-depth intraslab earthquakes and arc volcanism as physical expressions of crustal and uppermost mantle metamorphism in subducting slabs. In: Bebout GE et al. (eds) *Subduction: top to bottom*. Geophysical Monograph Series, vol 96. AGU, Washington, DC, pp 195–214
- Klotz J, Abolghasem A, Khazaradze G, Heinze B, Vietor T, Hackney R, Bataille K, Maturana R, Viramonte J, Perdomo R (2006) Long-term signals in the present-day deformation field of the central and Southern Andes and constraints on the viscosity of the Earth's Upper Mantle. In: Oncken O et al. (eds) *The Andes: active subduction orogeny, frontiers in earth sciences*. Springer, Berlin, pp 65–89
- Krawczyk CM, Mechie J, Tašárová Z, Lüth S, Stiller M, Brasse H, Echtler H, Bataille K, Wigger P, Araneda M (2006) Geophysical signatures and active tectonics at the South-Central Chilean Margin. In: Oncken O et al. (eds) *The Andes: active subduction orogeny, frontiers in earth sciences*. Springer, Berlin, pp 171–192
- Lamb S, Davis P (2003) Cenozoic climate change as a possible cause for the rise of the Andes. *Nature* 425:792–797

- Lara LE, Naranjo JA, Moreno H (2004) Rhyodacitic fissure eruption in Southern Andes (Cordón Caulle; 40.5°S) after the 1960 (Mw:9.5) Chilean earthquake: a structural interpretation. *J Volc Geotherm Res* 138:127–138
- Lezaeta P (2001) Distortion analysis and 3-D modeling of magnetotelluric data in the Southern Central Andes. PhD thesis, FU Berlin
- Lezaeta P, Brasse H (2001) Electrical conductivity beneath the volcanoes of the NW Argentinian Puna. *Geophys Res Lett* 28:4651–4654
- Lezaeta P, Muñoz M, Brasse H (2000) Magnetotelluric image of the crust and upper mantle in the backarc of the NW Argentinean Andes. *Geophys J Int* 142:841–854
- Li Y (2002) A finite element algorithm for electromagnetic induction in two-dimensional anisotropic conductivity structures. *Geophys J Int* 148:389–401
- López-Escobar L, Cembrano J, Moreno H (1995) Geochemistry and tectonics of the Chilean Southern Andes basaltic Quaternary volcanism (37–46°S). *Rev Geol Chile* 22:219–234
- Lüth S, Wigger P (2003) A crustal model along 39°S from a seismic refraction profile – ISSA 2000. *Rev Geol Chile* 30:83–101
- MacKenzie L, Abers GA, Fischer KM, Syracuse EM, Protti JM, Gonzalez V, Strauch W (2008) Crustal structure along the southern Central American volcanic front. *Geochem Geophys Geosyst* 9:Q08S09. doi:10.1029/2008GC001991
- Mackie RL, Smith JT, Madden TR (1994) Three-dimensional modeling using finite difference equations: the magnetotelluric example. *Radio Sci* 29:923–935
- Mann P, Rogers RD, Gahagan L (2007) Overview of plate tectonic history and its unresolved tectonic problems. In: Bundschuh J, Alvarado GE (eds) *Central America: geology, resources, hazards*, vol 1. Taylor & Francis, London, pp 201–238
- McNeice GW, Jones AG (2001) Multi-site, multi-frequency tensor decomposition of magnetotelluric data. *Geophysics* 66:158–173
- Melnick D, Rosenau M, Folguera A, Echtler H (2006) Neogene tectonic evolution of the Neuquén Andes western flank (37–39°S). In: Kay SM, Ramos VA (eds) *Evolution of an Andean margin: a tectonic and magmatic view from the Andes to the Neuquén Basin (35–39°S)*. *Geol Soc Am Spec Paper* 407. doi:10.1130/2006.2407(04)
- Mibe K, Fujii T, Yasuda A (1999) Control of the location of the volcanic front in island arcs by aqueous fluid connectivity in the mantle wedge. *Nature* 401:259–262
- Montahei M (2011) Investigation of electrically anisotropic structures employing magnetotelluric data. PhD thesis, University of Tehran
- Müller A, Haak V (2004) 3-D modeling of the deep electrical conductivity of Merapi volcano (Central Java): integrating magnetotellurics, induction vectors and the effects of steep topography. *J Volc Geotherm Res* 138:205–222
- Muñoz N, Charrier R (1996) Uplift of the western border of the Altiplano on a west-vergent thrust system, Northern Chile. *J South Am Earth Sci* 9:171–181
- Muñoz J, Troncoso R, Duhart P, Crignola P, Farmer L, Stern CR (2000) The relation of the mid-Tertiary coastal magmatic belt in south-central Chile to the late Oligocene increase in plate convergence rate. *Rev Geol Chile* 27:177–203
- Myers SC, Beck S, Zandt G, Wallace T (1998) Lithospheric-scale structure across the Bolivian Andes from tomographic images of velocity and attenuation for P and S waves. *J Geophys Res* 103:21233–21252
- Nakamura K (1977) Volcanoes as possible indicators of tectonic stress orientation (principle and proposal). *J Volcan Geotherm Res* 2:1–16
- Nesbitt BE (1993) Electrical resistivities of crustal fluids. *J Geophys Res* 98:4301–4310
- Parada MA, López-Escobar L, Oliveros V, Fuentes F, Morata D, Calderón M, Aguirre L, Féraud G, Espinoza F, Moreno H, Figueroa O, Muñoz J, Troncoso Vásquez R, Stern CR (2007) Andean magmatism. In: Moreno T, Gibbons W (eds) *The geology of Chile*. Geological Society, London, pp 115–146
- Pek J, Verner T (1997) Finite difference modelling of magnetotelluric fields in 2-D anisotropic media. *Geophys J Int* 128:505–521
- Patro PK, Egbert GD (2008) Regional conductivity structure of Cascadia: preliminary results from 3D inversion of USArray transportable array magnetotelluric data. *Geophys Res Lett* 35:L20311. doi:10.1029/2008GL035326
- Peacock SM, van Keken PE, Holloway SD, Hacker BR, Abers GA, Ferguson RL (2005) Thermal structure of the Costa Rica-Nicaragua subduction zone. *Phys Earth Planet Int* 149:187–200
- Pizarro D (1993) Los pozos profundos perforados en Costa Rica: aspectos litológicos y bioestratigráficos. *Rev Geol Am Central* 15:81–85
- Protti M, Guendel F, McNally K (1995) Correlation between the age of the subducting Cocos plate and the geometry of the Wadati-Benioff zone under Nicaragua and Costa Rica. *Geol Soc Am Spec Paper* 295:309–326
- Ramos VA, Kay SM (2006) Overview of the tectonic evolution of the southern Central Andes of Mendoza and Neuquén (35°–39°S latitude). In: Kay SM, Ramos VA (eds) *Evolution of an Andean margin: a tectonic and magmatic view from the Andes to the Neuquén Basin (35°–39°S)*. Geological Society of America Special Paper, vol 407. doi:10.1130/2006.2407(01)
- Ranero CR, Phipps Morgan J, McIntosh K, Reichert C (2003) Bending-related faulting and mantle serpentinization at the Middle America trench. *Nature* 425:367–373
- Reuther CD, Moser E (2007) Orientation and nature of active crustal stresses determined by electromagnetic measurements in the Patagonian segment of the South America Plate. *Int J Earth Sci (Geol. Rundschau)*. doi:10.1007/s00531-007-0273-0
- Rietbrock A, Haberland C, Bataille K, Dahm T, Oncken O (2005) Studying the seismogenic coupling zone with a passive seismic array. *EOS Trans AGU* 86:293
- Ritz M, Bondoux F, Hérail G, Sempere T (1991) A magnetotelluric survey in the northern Bolivian Altiplano. *Geophys Res Lett* 18:475–478
- Roberts JJ, Tyburczy JA (1999) Partial-melt electrical conductivity: Influence of melt composition. *J Geophys Res* 104:7055–7065
- Rodi W, Mackie RL (2001) Nonlinear conjugate gradients algorithm for 2-D magnetotelluric inversions. *Geophysics* 66:174–187
- Rosenau M, Melnick D, Echtler H (2006) Kinematic constraints on intra-arc shear and strain partitioning in the

- southern Andes between 38°S and 42°S latitude. *Tectonics* 25. doi:10.1029/2005TC001943
- Rüpke LH, Morgan JP, Hort M, Connolly JAD (2002) Are the regional variations in Central American arc lavas due to differing basaltic versus peridotitic slab sources of fluids? *Geology* 30:1035–1038
- Rychert CA, Fischer KM, Abers GA, Plank T, Syracuse EM, Protti JM, Gonzalez V, Strauch W (2008) Strong along-arc variations in attenuation in the mantle wedge beneath Costa Rica and Nicaragua. *Geochem Geophys Geosyst* 9:Q10S10. doi:10.1029/2008GC002040
- Sallarès V, Dañobeitia JJ, Flueh ER (2001) Lithospheric structure of the Costa Rican Isthmus: effects of subduction zone magmatism on an oceanic plateau. *J Geophys Res* 106:621–643
- Scambelluri M, Philippot P (2001) Deep fluids in subduction zones. *Lithos* 55:213–227
- Scherwath M, Flueh E, Grevenmeyer I, Tilmann F, Contreras-Reyes E, Weinrebe W (2006) Investigating subduction zone processes in Chile. *EOS Trans AGU* 87:265
- Scheuber E, Bogdanic T, Jensen A, Reutter K-J (1994) Tectonic development of the north Chilean Andes in relation to plate convergence and magmatism since the Jurassic. In: Reutter K-J, Scheuber E, Wigger P (eds) *Tectonics of the Southern Central Andes*. Springer, Berlin, pp 121–140
- Scheuber E, Mertmann D, Ege H, Silva-González P, Heubeck C, Reutter K-J, Jacobshagen V (2006) Exhumation and basin development related to formation of the Central Andean Plateau, 21°S. In: Oncken O et al. (eds) *The Andes: active subduction orogeny, frontiers in earth sciences*. Springer, Berlin, pp 459–474
- Schilling FR, Trumbull RB, Brasse H, Haberland C, Asch G, Bruhn D, Mai K, Haak V, Giese P, Muñoz M, Ramelow J, Rietbrock A, Ricaldi E, Vietor T (2006) Partial melting in the Central Andean crust: a review of geophysical, petrophysical, and petrologic evidence. In: Oncken O et al. (eds) *The Andes: active subduction orogeny, frontiers in earth sciences*. Springer, Berlin, pp 459–474
- Schmidt MW, Poli S (1998) Experimentally based water budgets for dehydrating slabs and consequences for arc magma generation. *Earth Planet Sci Lett* 163:361–379
- Schmucker U (1970) Anomalies of geomagnetic variations in the Southwestern United States. *Bull Scripps Institution La Jolla, University of California Press, Los Angeles*
- Schmucker U, Forbush SE, Hartmann O, Giesecke AA, Casaverde M, Castillo J, Salgueiro R, del Pozo S (1966) Electrical conductivity anomaly under the Andes. *Carnegie Inst Wash Yearb* 65:11–28
- Schurr B, Asch G, Rietbrock A, Trumbull R, Haberland C (2003) Complex patterns of fluid and melt transport in the central Andean subduction zone revealed by attenuation tomography. *Earth Planet Sci Lett* 215:105–119
- Schwalenberg K, Haak V, Rath V (2002) The application of sensitivity studies on a two-dimensional resistivity model from the Central Andes. *Geophys J Int* 150:673–686
- Schwarz G, Krüger D (1997) Resistivity cross section through the southern central Andes as inferred from magnetotelluric and geomagnetic deep soundings. *J Geophys Res* 102:11957–11978
- Sempere T, Hérail G, Oller J, Bonhomme MG (1990) Late Oligocene-early Miocene major tectonic crisis and related basins in Bolivia. *Geology* 18:946–949
- Shaw H (1980) Fracture mechanisms of magma transport from the mantle to the surface. In: Hargraves RB (ed) *Physics of magmatic processes*. Princeton University Press, Princeton, NJ
- Sick C, Yoon M-K, Rauch K, Buske S, Lüth S, Araneda M, Bataille K, Chong G, Giese P, Krawczyk C, Mechie J, Meyer H, Oncken O, Reichert C, Schmitz M, Shapiro S, Stiller M, Wigger P (2006) Seismic images of accretive and erosive subduction zones from the Chilean margin. In: Oncken O et al. (eds) *The Andes: active subduction orogeny, frontiers in earth sciences*. Springer, Berlin, pp 147–169
- Siemon B (1997) An interpretation technique for superimposed induction anomalies. *Geophys J Int* 130:73–88
- Simpson F, Bahr K (2005) *Practical magnetotellurics*. Cambridge University Press, Cambridge
- Smith JT (1995) Understanding telluric distortion matrices. *Geophys J Int* 122:219–226
- Smith JT (1997) Estimating galvanic-distortion magnetic fields in magnetotellurics. *Geophys J Int* 130:65–72
- Soyer W (2002) Analysis of geomagnetic variations in the Central and Southern Andes. PhD thesis, FU Berlin
- Soyer W, Brasse H (2001) Investigation of anomalous magnetic field variations in the central Andes of N Chile and SW Bolivia. *Geophys Res Lett* 28:3023–3026
- Soyer W, Unsworth M (2006) Deep electrical structure of the northern Cascadia (British Columbia, Canada) subduction zone: implications for the distribution of fluids. *Geology* 34. doi:10.1130/G21951.1
- Springer M, Förster A (1998) Heat-flow density across the Central Andean subduction zone. *Tectonophysics* 291:123–139
- Stern CR (2004) Active Andean volcanism: its geologic and tectonic setting. *Rev Geol Chile* 31:161–206
- Sylvester AG (1988) Strike-slip faults. *Geol Soc Am Bull* 100:1666–1703
- Syracuse EM, Abers GA, Fischer K, MacKenzie L, Rychert C, Protti JM, González V, Strauch W (2008) Seismic tomography and earthquake locations in the Nicaraguan and Costa Rican upper mantle. *Geochem Geophys Geosyst* 9:Q07S08. doi:10.1029/2008GC001963
- Tassara A, Götze HJ, Schmidt S, Hackney R (2006) Three-dimensional density model of the Nazca plate and the Andean continental margin. *J Geophys Res* 111. doi:10.1029/2005JB003976
- Tatsumi Y (2003) Some constraints on arc magma genesis. In: Eiler J (ed) *Inside the subduction factory*. Geophysical Monograph Series, vol 138. AGU, Washington, DC, pp 277–292
- Tyburczy JA, Fislir DK (1995) Electrical properties of minerals and melts, mineral physics & crystallography. In: Ahrens TJ *Handbook of physical constants*, American Geophysical Union, Washington, DC, pp 185–208
- Vanyan LL, Berdichevsky MN, Pushkarev PYu, Romanyuk TV (2002) A geoelectric model of the Cascadia subduction zone. *Izvestiya Phys Solid Earth* 38:816–845
- Varentsov IvM, Golubev NG, Gordienko VV, Sokolova EYu (1996) Study of deep geoelectrical structure along EMSLAB Lincoln-Line. *Izvestiya Phys Solid Earth* 32:375–393
- Völker D, Wiedicke M, Ladage S, Gaedicke C, Reichert C, Rauch K, Kramer W, Heubeck C (2006) Latitudinal variation in sedimentary processes in the peru-Chile trench off Central

- Chile. In: Oncken O et al. (eds) *The Andes: active subduction orogeny, frontiers in earth sciences*. Springer, Berlin, pp 193–216
- von Huene R, Weinrebe W, Heeren F (1999) Subduction erosion along the North Chile margin. *Geodynamics* 27:345–358
- Walther CHE, Flueh ER, Ranero CR, von Huene R, Strauch W (2000) Crustal structure across the Pacific margin of Nicaragua: evidence for ophiolitic basement and a shallow mantle sliver. *Geophys J Int* 141:759–777
- Wannamaker PE (1999) Affordable Magnetotellurics: interpretation in Natural Environments. In: Oristaglio M, Spies B (eds) *Three-dimensional electromagnetics*. Soc. Expl. Geophys., Tulsa, pp 349–374
- Wannamaker PE, Booker JR, Jones AG, Chave AD, Filloux JH, Waff HS, Law LK (1989) Resistivity cross-section through the Juan de Fuca subduction system and its tectonic implications. *J Geophys Res* 94:14127–14144
- Wannamaker PE, Caldwell TG, Jiracek GR, Maris V, Hill GJ, Ogawa Y, Bibby HM, Bennie SL, Heise W (2009) Fluid and deformation regime of an advancing subduction system at Marlborough. New Zealand. *Nature* 460. doi:10.1038/nature08204
- Weidelt P (1999) 3-D Conductivity models: implications of electrical anisotropy. In: Oristaglio M, Spies B (eds) *Three-dimensional electromagnetics*. Society of Exploration Geophysicists, Tulsa, pp 119–137
- Wessel P, Smith WHF (1998) New, improved version of the Generic Mapping Tools released. *EOS Trans AGU* 79:579
- Whitman D, Isacks BL, Kay SM (1996) Lithospheric structure and along-strike segmentation of the Central Andean Plateau: seismic Q, magmatism, flexure, topography and tectonics. *Tectonophysics* 259:29–40
- Wiese H (1962) Geomagnetische Tiefentellurik Teil II: Die Streichrichtung der Untergrundstrukturen des elektrischen Widerstandes, erschlossen aus geomagnetischen Variationen. *Pageoph* 52:83–103
- Wigger P, Schmitz M, Araneda M, Asch G, Baldzuhn S, Giese P, Heinsohn W-D, Martínez E, Ricaldi E, Röwer P, Viramonte J (1994) Variation of the crustal structure of the southern Central Andes deduced from seismic refraction investigations. In: Reutter K-J, Scheuber E, Wigger P (eds) *Tectonics of the Southern Central Andes*. Springer, Berlin, pp 23–48
- Wörner G, Hammerschmidt K, Henjes-Kunst F, Lezaun J, Wilke H (2000) Geochronology (^{40}Ar - ^{39}Ar , K-Ar-, and He-exposure-ages) of Cenozoic magmatic rocks from Northern Chile (18°–22°S): implications for magmatism and tectonic evolution of the central Andes. *Rev Geol Chile* 27: 205–240
- Wörner G, Uhlig D, Kohler I, Seyfried H (2002) Evolution of the West Andean Escarpment at 18°S (N. Chile) during the last 25 Ma: uplift, erosion and collapse through time. *Tectonophysics* 345:183–198
- Yuan X, Asch G, Bataille K, Bock G, Bohm M, Echtler H, Kind R, Oncken O, Wölbern I (2006) Deep seismic images of the southern Andes. In: Kay SM, Ramos VA (eds) *Evolution of an Andean margin: a tectonic and magmatic view from the Andes to the Neuquén Basin (35°–39°S lat)*, Geological Society of American, Special paper. doi:10.1130/2006.2407(03)
- Yuan X, Sobolev SV, Kind R (2002) Moho topography in the central Andes and its geodynamic implications. *Earth Planet Sci Lett* 199:389–402
- Zhdanov MS (2009) *Geophysical Electromagnetic theory and methods*. Methods in geochemistry and geophysics, 43. Elsevier, 868pp